Ions

R. Nagaoka
Synchrotron SOLEIL, Saint-Aubin, France

Abstract
Ions are generated in a storage ring through collisions of a stored beam with residual gases. Their formation and influence on a stored beam are discussed including the so-called two-beam instability. Several methods for alleviating the ion effects are described.

Keywords
Storage ring; ions; beam dynamics; collective effects; beam instability; electromagnetic interactions.

1 Introduction

Ions are described in this lecture note as a source of disturbance to a beam stored in a storage ring. They are normally created via collisions of a stored beam with residual gases existing in the beam duct. Since some atomic electrons are ripped off through these electromagnetic (EM) interactions, ions are positively charged. They can be collectively repelled or attracted by the stored beam depending upon the sign of electric charge of the stored beam. Ions can induce a number of detrimental effects on the beam such as tune shifts, lifetime reduction and collective beam instability, all leading to a performance degradation of a storage ring.

Historically, ions caused performance limitations in both proton and electron rings. Many studies were carried out by various groups to understand the beam dynamics mechanisms of the encountered phenomena and thereby to explore means to avoid them [1–14]. In light-source storage rings where the stability of a circulating beam is of crucial importance, the serious impact of ions had led some machines, such as DCI, ACO, APS, and KEK-PF, to switch the stored beam from electrons to positrons [15]. As a general trend, a lower beam emittance is achieved in modern storage rings to raise the ring performance in terms of luminosity and brilliance. As a consequence, the trapping of ions in the electro-static potential of a stored beam that caused serious beam instabilities and suffered many rings in the past seems to have become much less of an issue. However, a new direct type of interactions between a stored beam and a beam of ions occurring in a single passage of the former may become a risk for future storage rings due to stronger electro-static field generated by the stored beam. Thus, ions could still be a potentially dangerous source of perturbation for modern and future storage rings.

The present paper is organized as follows. In the next section, we shall go through the basics of beam–ion dynamics, starting with the question of why we have ions in a storage ring. The impact of residual gases and ions on a stored beam, and ion motions due to the EM fields of the stored beam shall be discussed. In Section 3, we shall look at beam instabilities caused by ions. One type is due to trapped ions and the other is the so-called Fast Beam–Ion Instability (FBII). In Section 4, mitigation methods for ion effects shall be reviewed. Some specific examples of observing ion effects shall also be introduced. Conclusions are given in Section 5.

2 Basis of beam–ion dynamics

In this section we shall go through some of the basic physical mechanisms, notions, and studies developed in the past surrounding beam–ion dynamics, starting with asking us why ions are present in

https://doi.org/10.23730/CYRSP-2017-003.519

vacuum chambers. The influence of residual gases and ions on the stored beam, as well as ion motions due to the EM fields of the stored beam and magnets, shall be considered. It must be noted that the descriptions below benefited much from the earlier lecture notes on ions from the CAS series [16, 17], and in particular that of Sakanaka from the KEK-OHO accelerator school series [18].

2.1 Ultra-vacuum and residual gases

In reaching a maximal ring performance, ideally a stored beam should not get any disturbance in circulating along its closed orbit. This means that the beam duct needs be kept under excellent vacuum. With the vacuum technology of today applied to accelerators, we can reach the pressure level of the so-called Ultra-High Vacuum (UHV), which corresponds to lower than 10^{-9} mbar. Nonetheless, the residual gases in UHV could still become a significant source of beam perturbations. The principal mechanism is the collision of residual gases with beam, which specifically means elastic and inelastic EM scattering, causing particle losses and beam lifetime reduction. Through scattering, the residual gases could lose their atomic electrons and be ionized. Generated ions, as an ensemble, could then create an electrostatic potential and act on the beam both incoherently and coherently. We shall see more specifically below what kinds of interactions could take place.

The general trend today with modern storage rings in further raising their performance is to store an increasingly high intensity beam with lower emittance, which is often combined with the use of narrower beam ducts, such as for insertion devices and stronger quadrupole focusing. The lowering of vacuum conductance and the combination of elements mentioned above, bring about a number of reasons for which issues related to vacuum, and therefore to ions, still potentially remain the high concern for modern and future accelerators.

2.2 Collisions with residual gases

Let us consider the case of an electron colliding with residual gases. The collision can be classified into the following three categories (Fig. 1):

i) Møller scattering, which is elastic scattering with an atomic electron;

ii) Rutherford scattering, which is elastic scattering with the EM field of a nucleus;

iii) bremsstrahlung, which is inelastic scattering with the EM field of a nucleus converting a part of the electron's kinetic energy into EM radiation.

The total collision cross-section $\sigma_{\mathrm{Col}}^{\mathrm{Total}}$ of an atom with an atomic number Z_{i} is expressed as a sum of the three:

$$\sigma_{\mathrm{Col}}^{\mathrm{Total}} = Z_{\mathrm{i}} \cdot \sigma_{\mathrm{Møller}} + \sigma_{\mathrm{Rutherford}}(Z_i) + \sigma_{\mathrm{Bremsstrahlung}}(Z_i) \ . \tag{1}$$

Denoting the density of the concerned molecule by d_{m} and the velocity of the stored beam by βc, the collision rate is given by

$$\frac{1}{\tau_{\mathrm{Col}}} = \sigma_{\mathrm{Col}}^{\mathrm{Total}} \cdot d_{\mathrm{m}} \cdot \beta c \ , \tag{2}$$

where d_{m} is related to the partial pressure P_{m} at 20°C via $d_{\mathrm{m}}\,[\mathrm{m}^{-3}] = 2.47 \times 10^{22}\, P_{\mathrm{m}}\,[\mathrm{mbar}]$. In cases where the molecule consists of several atoms and/or there are several species in the residual gases, we take a sum of all contributions,

$$\frac{1}{\tau_{\mathrm{Col}}} = \sum_m \sum_k \frac{1}{(\tau_{\mathrm{Col}})_{mk}} , \tag{3}$$

where the index k is for different atoms in a molecule m and the index m is for molecule species.

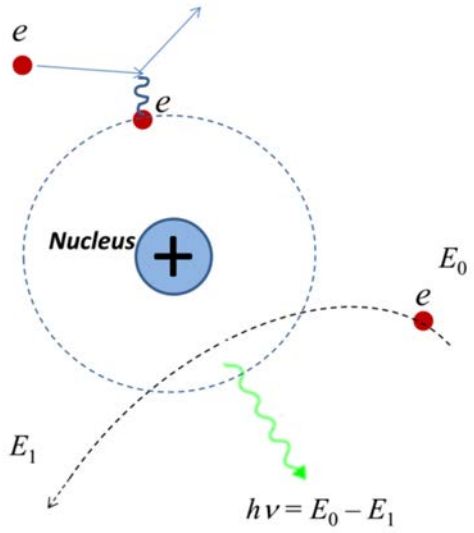

Fig. 1: Processes of collision of an electron with residual gases

2.3 Ionization of residual gases

In a similar way, we can obtain the ionization rate $1/\tau_{\mathrm{ion,m}}$ of a stored particle, or equivalently its ionization time $\tau_{\mathrm{ion,m}}$, by replacing $\sigma_{\mathrm{Col}}^{\mathrm{Total}}$ by the ionization cross-section $\sigma_{\mathrm{ion,m}}$ in the previous formula,

$$\frac{1}{\tau_{\mathrm{ion,m}}} = d_{\mathrm{m}} \cdot \sigma_{\mathrm{ion,m}} \cdot \beta c \ . \tag{4}$$

In general, $\sigma_{\mathrm{ion,m}}$ only depends on the species m and the velocity of the stored particle βc, as follows:

$$\sigma_{\mathrm{ion,m}} = 4\pi \left(\frac{\hbar}{m_{\mathrm{e}} c} \right)^2 \cdot (M^2 \cdot x_1 + C \cdot x_2) \ , \tag{5}$$

where m_{e} is the electron mass, the quantity

$$4\pi \left(\frac{\hbar}{m_{\mathrm{e}} c} \right)^2$$

equals 1.874×10^{-24} [m^2], x_1 and x_2 depend on β as

$$x_1 = \beta^2 \cdot \ln\left(\frac{\beta^2}{1-\beta^2}\right) - 1, \quad x_2 = \beta^2 \ ,$$

and M^2 and C are molecule dependent constants as shown in Table 1.

Table 1. Value of the constants M^2 and C for typical molecules.

Molecule	M^2	C	Z^a	A^b
H_2	0.5	8.1	2	2
N_2	3.7	34.8	14	28
CO	3.7	35.1	14	28
O_2	4.2	38.8	16	32
H_2O	3.2	32.3	10	18
CO_2	5.75	55.9	22	44
C_6H_4	17.5	162.4	46	76

[a]Atomic number; [b]mass number.

2.4 Beam-induced electromagnetic fields and their characteristics

Let us review the static EM field created by a round coasting beam of radius a and current I in a circular chamber of radius b (Fig. 2). Using the relation from Gauss's theorem,

$$\iint \vec{E}\cdot \mathrm{d}\vec{a} \;=\; \int \frac{\rho}{\varepsilon_0}\mathrm{d}V \quad ,$$

where ρ is the charge density and

$$\oint \vec{B}\cdot \mathrm{d}\vec{\ell} \;=\; \mu_0 I \;,$$

we get for the radial component of the electric field E_r,

$$E_r \;=\; \begin{cases} \dfrac{\mathrm{e}\lambda}{2\pi\varepsilon_0}\dfrac{r}{a^2} & (0<r<a) \\ \dfrac{\mathrm{e}\lambda}{2\pi\varepsilon_0}\dfrac{1}{r} & (a<r) \end{cases} \quad , \tag{6}$$

and the azimuthal component of the magnetic field B_φ,

$$B_\varphi \;=\; \begin{cases} \dfrac{\mu_0 I}{2\pi a^2}\cdot r & (0<r<a) \\ \dfrac{\mu_0 I}{2\pi r} & (a<r) \end{cases} \quad , \tag{7}$$

where $\lambda = I/(\mathrm{e}\beta c)$ is the line density of the electron beam and βc is the speed of the electrons. Since an ion charged to +1e having a longitudinal speed of $\beta_i c$ gets a force from the EM field of $F_r^E = \mathrm{e}E_r$ and $F_\varphi^B = \mathrm{e}\beta_i c B_\varphi$, we find from Eqs. 6 and 7 that for all values of r,

$$\frac{F_r^B}{F_r^E} \;=\; \beta_i\beta \;\cong\; \beta_i \;\ll\; 1 \;,$$

as ions are relatively heavy and move slowly. This leads to the fact the magnetic force F_{φ}^{B} of the stored beam can usually be ignored as compared to the electric field F_{r}^{E}.

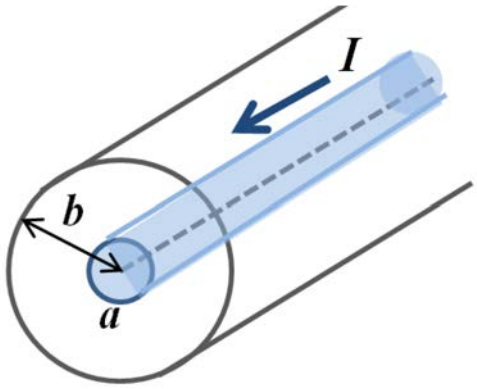

Fig. 2: A coasting beam of radius *a* and current *I* in a beam pipe of radius *b*

2.5 Ion trapping: Coasting beam

Using the static electric field E_r created by the beam (Eq. 6), the electric potential created by a coasting beam can be straightforwardly calculated as given by

$$V(r) = -\int_{b}^{r} E_r \, \mathrm{d}r = \begin{cases} \dfrac{\mathrm{e}\lambda}{2\pi\varepsilon_0}\left(\dfrac{r^2}{2a^2} - \dfrac{1}{2} + \ln\dfrac{a}{b}\right) & (0 < r < a) \\ \dfrac{\mathrm{e}\lambda}{2\pi\varepsilon_0}\cdot\ln\dfrac{r}{b} & (a < r) \end{cases} . \qquad (8)$$

Evaluating the depth of the potential for realistic cases (see Fig. 3), we find that the ions having only a thermal energy in the order of $k_B T$ (~10^{-21} J) cannot escape from the potential, the value of which is of the order of some tens of volt (and therefore an energy of ~10^{-18} J). The other important feature to be noted is that the potential depth increases as the beam emittance decreases and the beam intensity increases. A beam potential calculated for the ISR ring is shown in Fig. 4. Locations of clearing electrodes are indicated by dots [17].

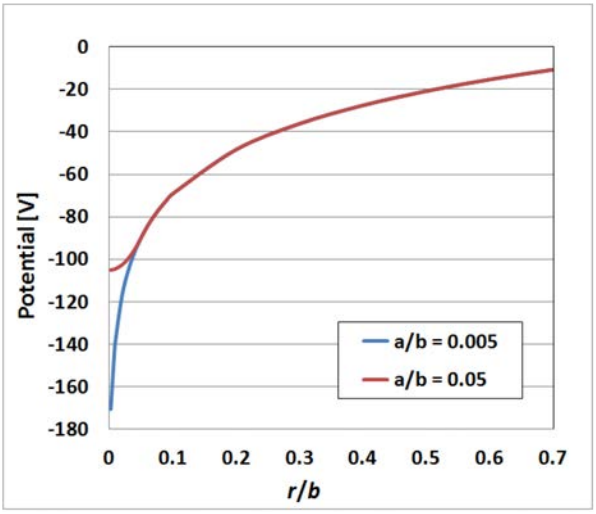

Fig. 3: Static electrostatic potential $V(r)$ created by a beam of radius *a*. The values for the parameters λ and *b* were taken from SOLEIL (I = 500 mA and b = 0.0125 m).

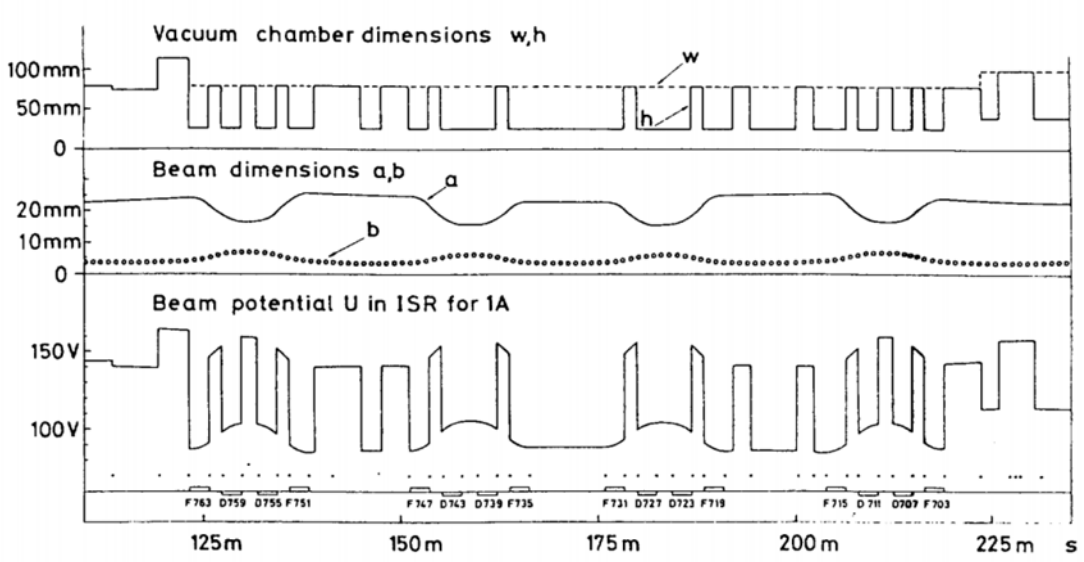

Fig. 4: Evaluation of the beam-induced electrostatic potential in ISR. The locations of clearing electrodes are indicated by dots. Taken from Ref. [17].

2.6 Neutralization

As the trapping of ions progresses, the potential depth decreases due to neutralization of opposing charges, which saturates the trapping process. The degree of neutralization is defined by

$$\eta = \frac{N_i}{N} , \tag{9}$$

where N_i and N are the total number of ions and electrons in the ring, respectively. If all ions are +1e charged, then $0 \leq \eta \leq 1$. For a proton ring, on the contrary, the electrons created by ionization could be trapped. Instead, ions could be repelled by the proton potential and bombard the chamber surface, which in turn induces outgassing. This could lead to a cascading phenomenon called the ‘pressure bump’.

2.7 Bassetti–Erskine formula

Analytical expressions for the transverse electric fields E_x and E_y created by an electron bunch having Gaussian distributions in the two transverse planes were derived by Bassetti and Erskine [19]. Since electron beams are usually Gaussian and since, in addition, the transverse ion distributions are often approximated as those of the stored beam, the Bassetti–Erskine formula is frequently used in evaluating the electric forces felt by the two beams. Starting from the Poisson equation,

$$\nabla^2 \phi = \frac{\rho}{\varepsilon_0} , \tag{10}$$

with the transverse charge distribution function ρ given by

$$\rho(x,y) = \frac{Q}{2\pi\sigma_x\sigma_y} \cdot \exp\left[-\left(\frac{x^2}{2\sigma_x^2} + \frac{y^2}{2\sigma_y^2} \right) \right] \tag{11}$$

where Q represents the total charge over the transverse distribution of a bunch, and σ_x and σ_y are the RMS values of the Gaussian distributions, the potential ϕ was solved analytically by assuming $\sigma_x > \sigma_y$ in an integral form. It then follows that the electric field satisfies

$$E_x - \mathrm{i}E_y = -\mathrm{i}\frac{Q}{2\varepsilon_0\sqrt{2\pi(\sigma_x^2-\sigma_y^2)}}\cdot\left\{w(a+\mathrm{i}b) - \mathrm{e}^{[-(a+\mathrm{i}b)^2+(ar+\mathrm{i}b/r)^2]}\cdot w(ar+\mathrm{i}b/r)\right\} \quad (12)$$

with the parameters a, b, and r given by

$$a = \frac{x}{\sqrt{2(\sigma_x^2-\sigma_y^2)}},\quad b = \frac{y}{\sqrt{2(\sigma_x^2-\sigma_y^2)}}\ ,\ \text{and}\ \ r = \frac{\sigma_y}{\sigma_x}\ ,$$

and $w(z)$ is the complex error function. The two transverse electric field components can consequently be expressed by

$$E_x = \frac{Q}{2\pi\varepsilon_0\sigma_x(\sigma_x+\sigma_y)}\cdot x + \text{higher-order terms}, \quad (13a)$$

$$E_y = \frac{Q}{2\pi\varepsilon_0\sigma_y(\sigma_x+\sigma_y)}\cdot y + \text{higher-order terms} \quad (13b)$$

,

respectively. Derivations for the case $\sigma_x < \sigma_y$ can similarly be made.

2.8 Ion trapping: Bunched beam

Let us now consider ion trapping with a bunched beam. With bunched beams, ions are only attracted during the passage of a bunch, and drift freely in between two bunches (in places where there are no magnets) (Fig. 5). Transverse motions of an ion thus resemble those of a circulating electron. Their stability (i.e. trapping) can be argued using transfer matrices in the linear approximation. Consider the vertical motion of an (+1e charged) ion in a symmetric beam filling. During the passage of a bunch, Newton's equation for an ion reads

$$M_{\mathrm{ion}}\ddot{y}_{\mathrm{i}} = \mathrm{e}E_y^{\mathrm{e}} = -\mathrm{e}\frac{Q}{2\pi\varepsilon_0\sigma_y(\sigma_x+\sigma_y)}\cdot y_{\mathrm{i}} = -\frac{N}{n_{\mathrm{b}}L_{\mathrm{b}}}\frac{2r_{\mathrm{p}}c^2m_{\mathrm{p}}}{\sigma_y(\sigma_x+\sigma_y)}\cdot y_i \quad (14)$$

,

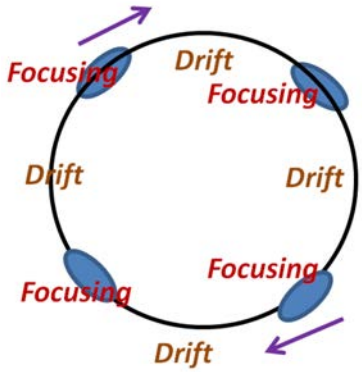

Fig. 5: The focusing system seen by an ion in a storage ring. Circulating electron bunches act as focusing quadrupoles and spacing between them as drifts.

where the double dot signifies a double derivative with respect to the time variable, $M_{\mathrm{ion}} = A \cdot m_{\mathrm{p}}$, where A is the mass number of the ions, N denotes the total number of stored electrons, n_{b} is the number of bunches, r_{p} is the classical proton radius (= $\mathrm{e}^2/4\pi\varepsilon_0 m_{\mathrm{p}}c^2$), L_{b} is the total bunch length, m_{p} is the proton mass, and E_y^{e} represents the vertical electric field created by the electron beam. In the familiar transfer matrix formulation, from the above linear equation of motion we have

$$\begin{pmatrix} y_{\mathrm{i}} \\ \dot{y}_{\mathrm{i}} \end{pmatrix}_{\mathrm{new}} = \begin{pmatrix} 1 & 0 \\ -a & 1 \end{pmatrix} \begin{pmatrix} y_{\mathrm{i}} \\ \dot{y}_{\mathrm{i}} \end{pmatrix}_{\mathrm{old}} , \tag{15}$$

during the passage of the electron beam. The focusing parameter a is given by

$$a = \frac{N}{n_{\mathrm{b}}} \frac{2 r_{\mathrm{p}} c}{\beta \sigma_y (\sigma_x + \sigma_y)} \frac{1}{A} \tag{16}$$

and β represents the relativistic factor corresponding to the speed of the stored electrons. The transfer matrix equation in between the passage of two bunches is that of a drift space

$$\begin{pmatrix} y_{\mathrm{i}} \\ \dot{y}_{\mathrm{i}} \end{pmatrix}_{\mathrm{new}} = \begin{pmatrix} 1 & \tau \\ 0 & 1 \end{pmatrix} \begin{pmatrix} y_{\mathrm{i}} \\ \dot{y}_{\mathrm{i}} \end{pmatrix}_{\mathrm{old}} , \tag{17}$$

where τ is given by $2\pi R/n_{\mathrm{b}}\beta c$ (where R is the ring radius).

2.9 Critical mass

The transfer matrix for one period, i.e. from the beginning of a bunch to the next, is therefore

$$M_{\mathrm{period}} = \begin{pmatrix} 1 & \tau \\ 0 & 1 \end{pmatrix} \cdot \begin{pmatrix} 1 & 0 \\ -a & 1 \end{pmatrix} . \tag{18}$$

The condition for any linear motions to be bounded $-2 \le Tr(M_{\mathrm{period}}) \le 2$ leads to

$$A \ge A_{\mathrm{c}} \equiv \frac{N}{n_{\mathrm{b}}} \frac{r_{\mathrm{p}}}{n_{\mathrm{b}}} \frac{\pi R}{\beta^2 \sigma_y (\sigma_x + \sigma_y)} . \tag{19}$$

The ion mass A_{c} defined by the above relation is called the critical mass. In this model we find that ions whose mass is lower than the critical mass cannot be trapped. It means that, as they are light, the focusing strength of the electron bunches deviates them too far away from the electron trajectory before the next bunch comes to attract them. The evidence of critical mass was experimentally observed in the 1.5 GeV electron–positron collider ADONE, in Frascati, Italy [20].

From Eq. 19, we can extract that ions have less chance of being trapped in a mode where there are few bunches, as A_{c} depends on the number of bunches as inversely square. Another aspect that is important is that the critical mass depends inversely on the product of the two sigmas, σ_x and σ_y, which in turn signifies that A_{c} effectively depends on the horizontal emittance as inversely square. This means that ions are much less likely to be trapped in a low-emittance ring. Again, the reason for this is the focusing of the electron beam being too strong when its transverse dimension is reduced, which kicks the ions away before the next bunch arrives. A numerical comparison showing the above dependence

of the critical mass on the number of bunches and the emittance has been made using the SOLEIL parameters (Fig. 6).

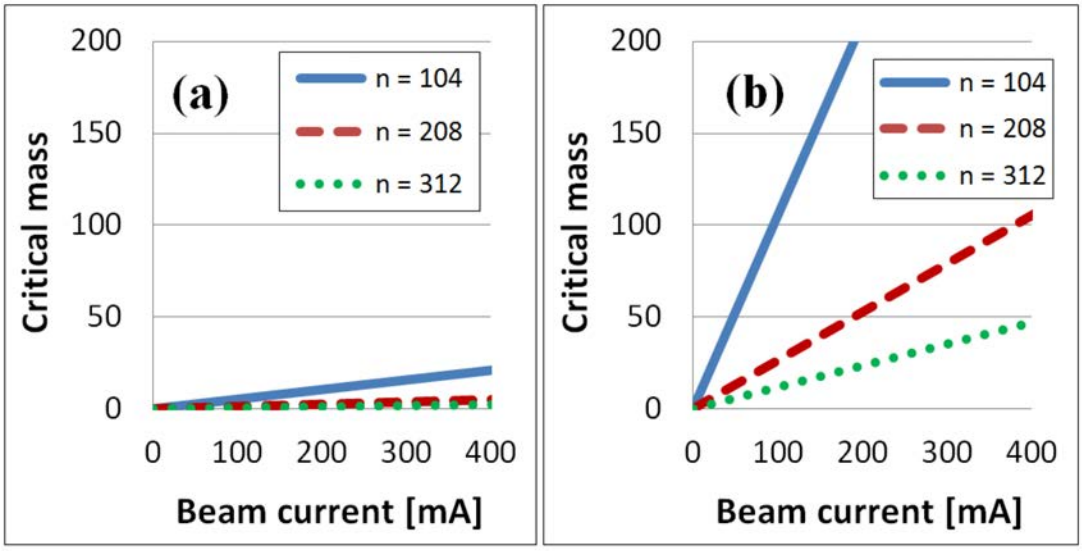

Fig. 6: Critical mass (Eq. 19) as a function of beam current for three symmetric beam fillings with different number of bunches. Machine parameters were taken from SOLEIL. Circumference = 354 m. (a) Horizontal emittance of 4 nm·rad (current value). (b) Horizontal emittance of 0.2 nm·rad (expected upgrade value). In both cases, the vertical emittance is assumed to be 1% of the horizontal value.

2.10 Betatron tune shifts

A cloud of trapped ions generally gives a transverse focusing force to the stored beam, inducing betatron tuneτ shifts $\Delta\nu_{x,y}$. They can be evaluated by the well-known formula

$$\Delta\nu = \frac{1}{4\pi}\oint \beta(s)\cdot\Delta k(s)\,\mathrm{d}s\ , \tag{20}$$

where $\beta(s)$ denotes the beta function, $\Delta k(s)$ represents the quadrupolar errors in a ring, and the integral over s is made around the ring. Assuming that the ions have the same Gaussian distributions as the electrons and are charged to +1e, we can use the Bassetti–Erskine formula (Eq. 13) to obtain the focusing strength $\Delta k_{\mathrm{i}}(s)$ due to ions as follows:

$$(\Delta k_{\mathrm{i}})_{x,y}(s) = \frac{1}{E_0/\mathrm{e}}\frac{\partial(E_{\mathrm{i}})_{x,y}}{\partial x,y} = \frac{1}{E_0/\mathrm{e}}\frac{d_{\mathrm{i}}}{\varepsilon_0}\cdot\frac{\mathrm{e}}{1+\sigma_{x,y}/\sigma_{y,x}}\ , \tag{21}$$

where d_{i} [m^{-3}] represents an ion density.

Similarly, the focusing strength $\Delta k_{\mathrm{SC}}(s)$ due to an electron beam's own space-charge force is given by

$$(\Delta k_{\mathrm{SC}})_{x,y}(s) = \frac{1}{\gamma^2}\frac{1}{E_0/\mathrm{e}}\frac{d_{\mathrm{e}}}{\varepsilon_0}\cdot\frac{\mathrm{e}}{1+\sigma_{x,y}/\sigma_{y,x}}\ , \tag{22}$$

where γ is the relativistic energy factor for the electrons and d_{e} [m^{-3}] is the electron density. Comparing the two tune shifts, we find that, since usually $\frac{d_{\mathrm{e}}}{d_{\mathrm{i}}}\cdot\frac{1}{\gamma^2}\ll 1$, we have $(\Delta\nu_{x,y}^{\mathrm{SC}})\ll(\Delta\nu_{x,y}^{\mathrm{ions}})$, namely, the

space charge tune shift is generally much smaller for a relativistic electron beam than that induced by ions.

2.11 Ion motions

When the ion mass A is much larger than the critical mass A_C, and if there are no magnetic fields, their drift motions between the passages of two successive bunches can be neglected. The resultant motions therefore become approximately harmonic oscillations,

$$\ddot{u}_i \approx -\omega_{iu}^2 u_i \ , \tag{23}$$

where

$$\omega_{iu}^2 = \frac{2\lambda r_p c^2}{A}\frac{1}{\sigma_u(\sigma_x+\sigma_y)} \quad (u = x, y) \ , \tag{24}$$

where $\lambda = I/(e\beta c)$ is the line density of the electrons. Inside a bending magnet where the magnetic field B is non-zero, the equations of ion motion then become

$$\begin{pmatrix} \ddot{s} \\ \ddot{x} \\ \ddot{y} \end{pmatrix} = \begin{pmatrix} 0 \\ -\omega_{ix}^2 \cdot x \\ -\omega_{iy}^2 \cdot y \end{pmatrix} + \omega_c \begin{pmatrix} -\dot{x} \\ \dot{s} \\ 0 \end{pmatrix} \ , \tag{25}$$

where ω_c is the cyclotron angular frequency given by eB/M_{ion}. The solution to the above equations are known to be off-centred sinusoidal motions for x and s at the frequency $\omega = \sqrt{\omega_{ix}^2 + \omega_c^2}$. In particular, ions drift *longitudinally* at the average speed of

$$< \dot{s} > = \left(\frac{\omega_{ix}}{\omega_c}\right)^2 \left[\omega_c \cdot x(0) + \dot{s}(0)\right] . \tag{26}$$

Ions generally tend to move longitudinally towards a minimum of the potential $V(r)$ of the stored beam. Since $V(0) = e\lambda/(2\pi\varepsilon_0)\cdot[\ln(a/b) - ½]$ (see Eq. (8)), they gather at locations in the ring where a/b is small (i.e. where the stored beam size is small and the chamber aperture is large), which are called the *neutralization spots*. It is considered effective to introduce ion-clearing electrodes at such positions.

2.12 Ion distributions

Many studies assume that ions created by the collision with the circulating beam have the same transverse distributions as the latter, which are usually Gaussian. The above assumption is correct regarding the initial ion distribution when ions are created. However, an equilibrium distribution reached under the beam electric potential turns out to be significantly different from the original Gaussian distribution due to the focusing force [21, 22]. Starting from the original Gaussian distribution with an RMS value given by that of the stored beam σ_e,

$$\rho(y) = \frac{1}{\sqrt{2\pi}\sigma_e}\cdot e^{-\frac{y^2}{2\sigma_e^2}} \ , \tag{27}$$

we find analytically in the linear regime that the ion distribution deforms to a distribution given by

$$\rho(y) = \frac{1}{\pi\sqrt{2\pi}\sigma_e} \cdot e^{-\frac{y^2}{4\sigma_e^2}} \cdot K_0\left(\frac{y^2}{4\sigma_e^2}\right), \tag{28}$$

where $K_0(z)$ is the zeroth-order modified Bessel function of the second kind (Fig. 7).

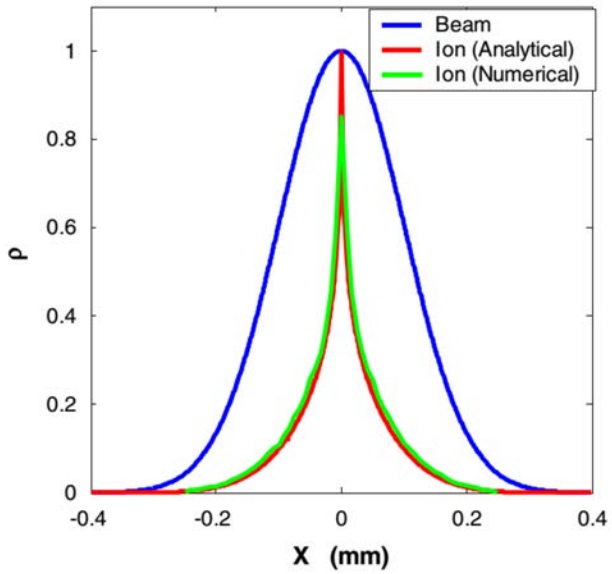

Fig. 7: Transverse distribution of an electron beam (Gaussian) and its corresponding ion distribution. For the ion distribution, a comparison is made between analytical (Eq. 28) and numerical results. Taken from Ref. 22.

Despite this fact, the conventional treatment of assuming a Gaussian distribution for the ions and applying the Bassetti–Erskine formula with the relation $\sigma_i = \sigma_e / \sqrt{2}$ turns out to closely reproduce the electric field created by the ions; a comparison is made in Fig. 8 [22].

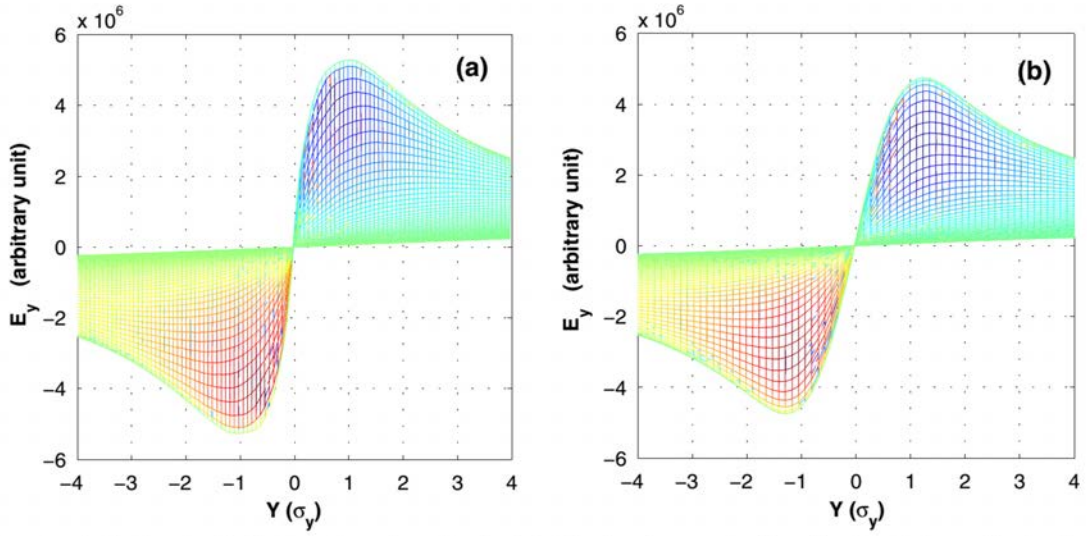

Fig. 8: Vertical electric field E_y of an ion cloud. (a) Obtained numerically via simulation. (b) A Gaussian distributed ion cloud with $\sigma_i = \sigma_e/\sqrt{2}$. The total charge is the same for the two distributions. Different lines in the figures are for different horizontal values of x. The coordinate Y is in the unit of rms beam size. Taken from Ref. [22].

2.13 Lifetime reduction and effective pressure rise due to trapped ions

When ions are trapped, they are populated on the stored beam trajectory whose distributions can be approximated as Gaussian as described previously with $\sigma_{ix} \sim \sigma_x / \sqrt{2}$ and $\sigma_{iy} \sim \sigma_y / \sqrt{2}$. If they are uniformly distributed in a ring, their density may be given by

$$d_{\mathrm{i}} = \frac{2N_{\mathrm{i}}}{\pi\sigma_x\sigma_y L}, \tag{29}$$

where L denotes the ring circumference. Using this localized density around the beam trajectory in the previous beam collision rate formula, we can estimate the lifetime reduction due to trapped ions,

$$\frac{1}{\tau_{\mathrm{ions}}} = \sigma_{\mathrm{Total}} \cdot d_{\mathrm{i}} \cdot \beta c \ . \tag{30}$$

Also, if we apply the relation d_{m} [m^{-3}] = 2.47 × 10^{22} P_{m} [mbar] introduced earlier, we can discuss the effective pressure rise due to trapped ions on the beam trajectory, as given by

$$P_{\mathrm{ions}}\ [\mathrm{mbar}] = \frac{1}{2.47\times10^{22}} \cdot \frac{2\eta N}{\pi\sigma_x\sigma_y L}, \tag{31}$$

where η is the neutralization factor defined by Eq. 9 and N is the total number of stored particles.

3 Two-beam instabilities

In this section, we shall look at beam instabilities that could occur between two beams that co-exist in the same ring, in which one is a circulating beam, and the other an ion beam. In accordance with the history, we shall first go through the case where the ion beam is trapped in the electrostatic potential of the circulating beam, which gave rise to a serious issue in many previous storage rings. We shall then look at the Fast Beam–Ion Instability (FBII), which could take place in a single passage of an electron beam. We attempt to learn about this by going through theoretical, numerical, and experimental studies made by the experts to understand the mechanisms of the instability. Readers interested in two-beam instabilities may also wish to follow the descriptions found in Ref. [23].

3.1 The case of trapped ions

Here we shall follow closely the descriptions made by Sakanaka in Ref. [18], where numerical studies were made to explain the experimental observations in the Photon Factory (PF) ring, running as a synchrotron radiation source at KEK. Indeed, instabilities due to trapped ions were serious issues at PF as well as some of the other light-source rings in the 1990s. With trapped ions, a resonant coupling between the two beams could arise that could lead to an instability and this type of instability was observed in many (second generation) light-source rings. The instability may consequently induce beam pulsation, as shown in Fig. 9, occurring at a frequency of around 20 Hz in the shown example, which is critically detrimental in a light source where the users request perfect stability of the photon beam. As we shall see below, the pulsation is a result of a beam blow-up due to interaction with ions, which is damped via radiation damping during the period when the ions are cleared, which is repeated periodically.

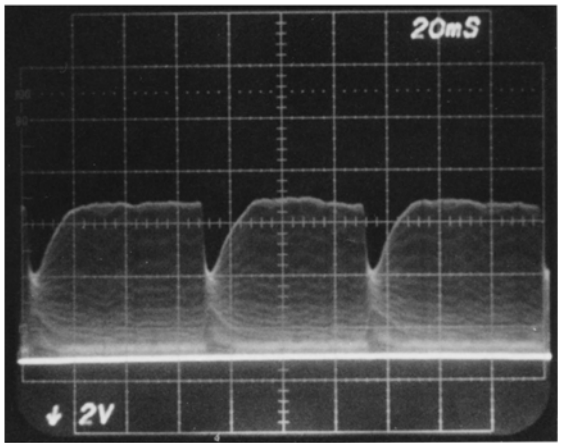

Fig. 9: Vertical beam pulsation observed at Photon Factory, KEK (horizontal unit: 20 ms/div). Taken from Ref. [18].

The beam instability can be described with a simplified model treating the Centre of Mass (CM) oscillations of the two beams [6, 12, 24, 25], by considering vertical oscillations alone, since the two beams interact primarily in this plane due to $\sigma_x > \sigma_y$ as also assumed above in Section 2. The model specifies furthermore that:

- An electron centre of mass y_{cme} oscillating in the ring with the $Q_{\beta y}\omega_0$ (where $Q_{\beta y}$ is the betatron tune) and under a linear force from the ion CM represented by the frequency ω_e;
- An ion centre of mass y_{cmi} feeling only a linear force from the electron CM represented by the frequency ω_i;
- Gaussian distributions for the two beams and +1e charge for ions (as in the descriptions above).

The corresponding coupled equations are

$$\begin{aligned} \ddot{y}_{\mathrm{cme}} + Q_{\beta y}^2\omega_0^2\, y_{\mathrm{cme}} &= -\omega_e^2 \cdot (y_{\mathrm{cme}} - y_{\mathrm{cmi}}) , \\ \ddot{y}_{\mathrm{cmi}} &= -\omega_i^2 \cdot (y_{\mathrm{cmi}} - y_{\mathrm{cme}}) , \end{aligned} \tag{32}$$

where

$$\omega_{\mathrm{e}}^2 = \frac{2\lambda_{\mathrm{i}} r_{\mathrm{e}} c^2}{\gamma} \frac{1}{\sigma_y(\sigma_x + \sigma_y)} , \tag{33}$$

$$\omega_{\mathrm{i}}^2 = \frac{2\lambda_{\mathrm{e}} r_{\mathrm{p}} c^2}{A} \frac{1}{\sigma_y(\sigma_x + \sigma_y)} , \tag{34}$$

where

$$r_{\mathrm{e}} = \frac{\mathrm{e}^2}{4\pi\varepsilon_0 m_{\mathrm{e}} c^2} ,$$

is the classical electron radius, and λ_{e} and λ_{i} are the line densities [m^{-3}] of electrons and ions, respectively. Solutions are searched in the form $y_{\mathrm{cme}} = A_{\mathrm{e}} \cdot \exp[\mathrm{i}(n\omega_0 - \omega)t + \mathrm{i}\theta_0]$ and $y_{\mathrm{cmi}} = A_{\mathrm{i}} \cdot \exp(-\mathrm{i}\omega t)$ by introducing a complex frequency ω. Inserting them into Eqs. 32, we get

$$(x^2 - Q_i^2)\cdot\left[(x-n)^2 - Q_y^2 - Q_e^2\right] \;=\; Q_e^2\cdot Q_i^2 \;, \tag{35}$$

where $x = \omega/\omega_0$, $Q_e = \omega_e/\omega_0$, and $Q_i = \omega_i/\omega_0$. If the solution consists of complex numbers, it always appears in the form $a \pm ib$ (where a, b are real), signifying that the two-beam motion is unstable. Numerical studies indicate that instability is likely to appear when n is just above the value of $Q_{\beta y}$.

Let us introduce here a study made at PF by applying the above model [18]. To have an idea of the case concerned, the major ring parameters are listed in Table 2. In Fig. 10 the real solutions at different beam currents are shown as a function of the neutralization factor $\delta = N_i/N$. Instability thresholds as a function of the vertical tune ν_y are shown in Fig. 11 for two values of δ for the case of $A = 2$ (H_2^+) and $A = 28$ (CO^+), and are compared with those measured. Comparisons with the experiments shown in the figure indicate that the employed two-centres-of-mass model describes the essential features of the dynamics.

Table 2. Main Photon Factory machine parameters

Parameter	Value
Energy E [GeV]	2.5
Circumference L [m]	187.07
Revolution frequency f_0 [MHz]	1.6026
Momentum compaction α	0.04
Horizontal emittance ε_x [m·rad]	$4.1\,\pi \times 10^{-7}$
Vertical emittance ε_y [m·rad]	$1.2\,\pi \times 10^{-8}$
Horizontal tune $Q_{\beta x}$	5.2–5.5
Vertical tune $Q_{\beta y}$	4.1–4.2
Horizontal damping time $\tau_{\beta x}$ [ms]	9.1
Vertical damping time $\tau_{\beta y}$ [ms]	7.8

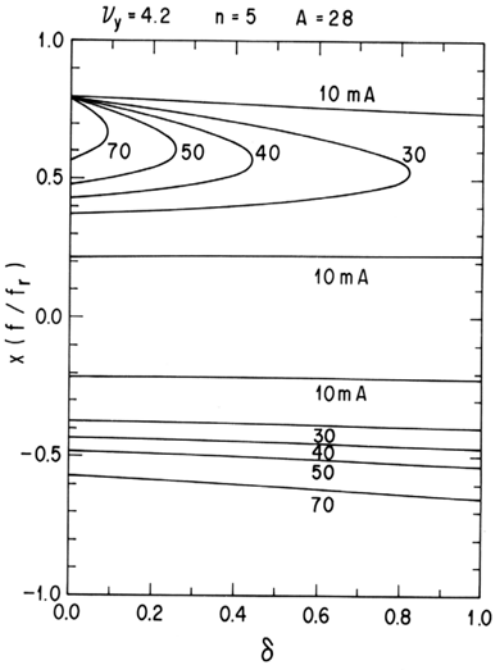

Fig. 10: Real solutions of Eq. (35) at different beam currents as a function of the neutralization factor $\delta = N_i/N$. Taken from Ref. [18].

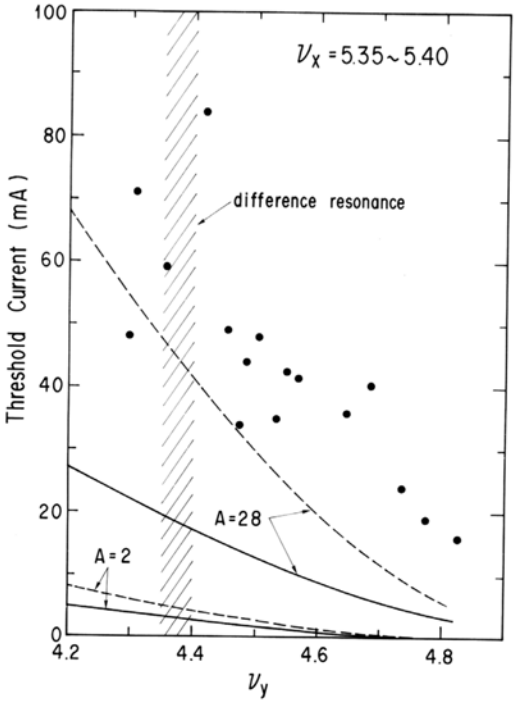

Fig. 11: Instability threshold versus vertical tune obtained from the solution of Eq. (35). Solid lines: δ = 1.0. Dashed lines: δ = 0.1. Black circles: Measured values. A = 28: CO^+. A = 2: H_2^+. Taken from Ref. [18].

3.2 Fast beam–ion instability

3.2.1 Linear model

We saw that the linear forces between the electron and ion beams represented by ω_e^2 and ω_i^2 depend linearly on the beam intensity and inversely linearly on the product of the transverse beam sizes $\sigma_y(\sigma_x + \sigma_y)$. For modern and future accelerators producing a high intensity and low emittance beam, the 'single-pass' interaction between the two beams may therefore become strong enough to jeopardize performance. In other words, even if ions are not trapped by the electrostatic potential of a stored electron beam, the two streams of beam could interact strongly in a single passage of the circulating beam. Even though the process of interaction for the ion beam is repeated from scratch at every turn, the perturbation upon the electron beam remains and thus could create a kind of resonance, which could eventually render the electron beam unstable. Upon such considerations, a linear theory and simulations were pioneered by Raubenheimer and Zimmermann [26]. This type of two-beam interaction resembles a 'beam breakup in linacs' and does not involve ion trapping. To understand the mechanism and the characteristics of this fast beam–ion instability, let us follow the essential features of the model developed by Raubenheimer and Zimmermann. The transverse coupled linear equations describing such a single-pass interaction of the two beams are given by

$$\frac{\mathrm{d}^2 y_\mathrm{b}(s,z)}{\mathrm{d}s^2} + \omega_\beta^2 \cdot y_\mathrm{b}(s,z) = K \cdot [y_\mathrm{i}(s,t) - y_\mathrm{b}(s,z)] \cdot \int_{-\infty}^{z} \rho(z')\mathrm{d}z' \,, \tag{36}$$

$$\frac{\mathrm{d}^2 \tilde{y}_\mathrm{i}(s,t)}{\mathrm{d}t^2} + \omega_\mathrm{i}^2 \cdot \tilde{y}_\mathrm{i}(s,t) = \omega_\mathrm{i}^2 \cdot y_\mathrm{b}(s,z) \,. \tag{37}$$

Three variables *s*, *z*, and *t* are used to describe the beam motions. A longitudinal position in the ring is specified by *s*, at which the electron beam may interact with ions. The relative position within the circulating electron beam is specified by *z*, with the definition $z = 0$ at the centre of the bunch train and extending in between $-z_0$ and $+z_0$, i.e. $-z_0 \le z \le +z_0$ (see Fig. 12). The head of the bunch train is defined as $z = -z_0$. Since the electron beam is assumed to be circulating at the speed of light *c*, the time variable *t* can be related to *s* via $t = (s + z)/c$.

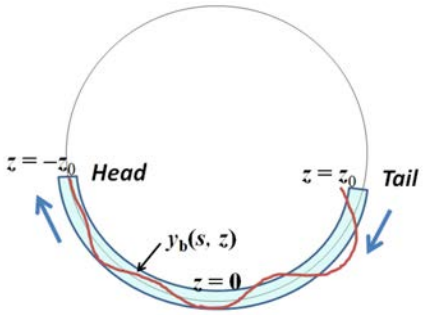

Fig. 12: The model, variables and coordinates assumed in the study of Fast Beam-Ion Instability (FBII) made in Ref. [26].

It must be noted that, in their original paper, the assumed accelerator is not restricted to a ring and could well be a transfer line. Also, the perturbing beam is not limited to ions and could be electrons against a positively charged beam. Reflecting the large difference in the mass between an ion and an electron, however, an ion frequency ω_i generally corresponds to an oscillation period that is much longer than the time spacing between bunches. The interaction between the two beams therefore becomes of a coupled-bunch nature, while in the case of electron clouds, the two-beam instability is usually of a single bunch nature.

In the first equation, $y_b(s,z)$ and $y_i(s,t)$ represent the electron and ion beam centroids, respectively. As in the model in Section 1.1, the non-perturbed motion of an electron beam centroid is a betatron oscillation represented by the oscillation constant ω_β ($= Q_{\beta y}\cdot\omega_0$). Like in the case of ion trapping, its motion is impacted by the electrostatic potential of ions, as represented by the constant *K*, corresponding to ω_e^2 in Eq. 32, its attractive force depending proportionally on the difference between the two amplitudes. What physically distinguishes this model from the previous one, however, is that, reflecting the single-pass ionization process, the amplitude of the ion perturbation depends explicitly on the number of electrons upstream the concerned electron beam centroid $y_b(s,z)$ at the relative position *z*, as indicated by the last factor on the right-hand side of Eq. 36. The longitudinal distribution of the electron bunch train (Fig. 12) is denoted by $\rho(z)$, which is normalized to unity.

The second equation (Eq. 37) describes the vertical centroid of a transverse slice of ions $\tilde{y}_i(s,t)$ created at a position *s* at a certain moment t' ($< -t$) due to the collision of electrons with the residual gases. Reflecting the way they are generated, the initial conditions $\tilde{y}_i(s,\, t'\,|\,t') = y_b(s,z')$ and $\mathrm{d}\tilde{y}_i(s,\, t'\,|\,t')/\mathrm{d}t = 0$ are adopted for a transverse slice. The ion-beam centroid $y_i(s,t)$ that influences the motion of an electron-beam centroid $y_b(s,z)$ consists of all possible ion slices $\tilde{y}_i(s,t\,|\,t')$ with $t' = (s+z')/c$ created at the position *s* until the time *t*. This is modelled as a $\rho(z)$-weighted average over z',

$$y_{\mathrm{i}}(s,t) \;=\; \frac{\int_{-\infty}^{z} \mathrm{d}z' + \rho(z')\cdot \tilde{y}_{\mathrm{i}}(s,\; t \mid s+z')}{\int_{-\infty}^{z} \rho(z')\mathrm{d}z'} \;. \tag{38}$$

Having well defined the model, the coupled equations are solved via perturbation expansion in K/ω_β. A great simplification in the mathematical derivation is obtained by assuming a rectangular distribution for ρ (z) as shown in Fig. 13, which assumes that there is no variation of the ion frequency ω_{i} along the bunch train. An asymptotic solution is derived in the form

$$y_{\mathrm{b}}(s,z) \;\approx\; \frac{\mathrm{e}^{2\sqrt{\eta}}}{\eta^{1/4}}\; \sin(\omega_{\mathrm{i}} z - \omega_\beta s + \theta - \phi) \;, \tag{39}$$

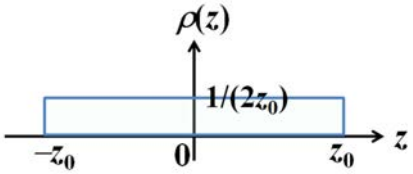

Fig. 13: A rectangular beam density distribution employed in Ref. [26]

where a variable η, given by

$$\eta \;\equiv\; \frac{K\cdot\omega_{\mathrm{i}}\cdot(z+z_0)^2 s}{16\omega_\beta z_0} \tag{40}$$

is assumed to be large ($\eta \;>>\; 1$) and θ and ϕ are constants appearing from the initial phases of oscillations. From the solution obtained above, the asymptotic growth rate evaluated at the tail of a bunch train $z = z_0$ (i.e. where the instability is strongest) is given by

$$\tau_{\mathrm{aymp}}^{-1}(s^{-1}) \;\;\approx\;\; \frac{N_{\mathrm{e}}^{3/2} n_{\mathrm{b}}^2}{\gamma} \times \left[5 p_{\mathrm{gas}}\;[\mathrm{Torr}]\; \frac{r_{\mathrm{e}} r_{\mathrm{p}}^{1/2} L_{\mathrm{sep}}^{1/2} c}{\sigma_y^{3/2}(\sigma_x+\sigma_y)^{3/2} A^{1/2}\omega_\beta} \right] , \tag{41}$$

where N_{e} is the number of electrons per bunch, n_{b} is the number of bunches, L_{sep} is the longitudinal spacing between bunches, and p_{gas} is the residual gas pressure in Torr. The formula is obtained for a horizontally flat electron beam.

As we see from Eq. (39), the asymptotic growth rate $\tau_{\mathrm{aymp}}^{-1}$ is obtained in the form

$$y_{\mathrm{b}}(s,z_0) \sim \mathrm{e}^{\sqrt{t/\tau_{\mathrm{asmp}}}}$$

and is therefore not an e-folding time. From Eq. (41), we understand that it depends strongly on the number of bunches ($\propto n_{\mathrm{b}}^2$), the number of particles per bunch ($\propto N_{\mathrm{e}}^{3/2}$) and the transverse beam sizes $(\propto\; \sigma_y^{-3/2}\cdot(\sigma_x+\sigma_y)^{-3/2})$. The assumed linear model is supposed to break down when the amplitude of the oscillation $y_{\mathrm{b}}(s,z)$ exceeds the vertical beam size σ_y where the coupling force between the two beam falls off. The growth rate above was evaluated for several existing rings in Ref. [25] (Table 3).

In particular, significantly short growth times result for ALS and the ESRF, i.e. in the light-source rings. However, no clear evidence of FBII was observed for these machines. The following points were therefore discussed as possible explanations.

i) The developed model assumes constant ω_i, whereas these light sources have strongly varying β functions due to adoption of double and triple bend achromat lattices. Namely, the ion frequency ω_i could effectively vary significantly around the ring.

ii) The presence of Landau damping sources such as strong sextupoles and non-zero chromaticity, which these rings generally possess.

iii) Other important nonlinear effects not considered in the linear model.

Table 3. Parameters and the asymptotic growth rates evaluated for several existing rings. Taken from Ref. [26].

Parameter	Accelerator					
	SLC arc	SLC e^+ DR	ALS	HERA e^-	CESR	ESRF
ε_x^N [m]	5×10^{-5}	3×10^{-5}	1.2×10^{-5}	2×10^{-3}	2.7×10^{-3}	7.5×10^{-5}
ε_y^N [m]	5×10^{-6}	3×10^{-6}	2×10^{-7}	1.1×10^{-4}	1.2×10^{-4}	7.5×10^{-6}
n_b	1	1	328	210	7	330
N_b	3.5×10^{10}	4×10^{10}	7×10^9	3.7×10^{10}	4.6×10^{11}	5×10^9
$\beta_{x,y}$ [m]	4	1,3	2.5,4	25	14,13	8,8
$\overline{\beta_y}$ [m]	4	3	4	25	13	8
σ_x [μm]	50	114	101	1000	2000	224
σ_y [μm]	15	62	17	230	400	70
z_0 [σ_z]	1 mm	5.9 mm	100 m	3024 m	335 m	140 m
E [GeV]	46	1.2	1.5	26	5	6
P [Torr]	10^{-5}	10^{-8}	10^{-9}	10^{-9}	5×10^{-9}	2×10^{-9}
Particle species	e^+	e^+	e^-	e^-	e^-	e^-
$\omega_{ion}/2\pi$ [MHz]	4×10^5	5×10^4	25	0.8	0.6	8.3
Single or multi-bunch	Single	Single	Multi-bunch	Multi-bunch	Multi-bunch	Multi-bunch
τ_{asym} [$z \approx z_0$]	1.1 μs	490 μs	2.4 μs	211 μs	3.9 ms	50 μs

3.2.2 Simulation of fast beam–ion instability

In addition to the linear model above, Raubenheimer and Zimmermann developed a simulation code to study numerically the growth of instability as a complementary and more rigorous method. The numerical simulation using macro-particles to represent the two beams (i.e. the strong–strong model) has indeed the large advantage of being able to integrate nonlinear effects, such as those due to finite beam sizes, and the capacity to follow self-consistently and dynamically the evolution of bunch distributions of the two beams. In the developed scheme, the ionization processes via the beam–residual gas collisions were simulated by using a specific ionization cross-section and partial pressure of a gas species to generate ions. The space-charge forces of each of the two beams were then calculated and applied to macro-particles of the opponent beam. The cascading process of ions growing in number due

to the successive arrival of electron bunches at the interaction point is rigorously treated. All ions at the end of each beam passage are discarded, assuming an ion-clearing beam gap from turn to turn. More specifically, the main features of the developed simulation are given below:

- Motions of macro-particles described with coordinates (x, x', y, y', $\delta E/E$);
- Beam bunches are initially Gaussian, longitudinally and transversely;
- Collision with gas takes place at some specified points in a ring (or a linac);
- A beam bunch is divided into ~five slices longitudinally;
- Each macro-particle is free to move in x and y according to the E-fields, but fixed in z;
- Two-dimensional grids (e.g. 25 × 25) with relation to the centre of mass of each slice introduced;
- At each grid:
  - Ions are created according to the specified pressure and collisional cross-section;
  - Ions have zero initial velocity;
  - The E-field of the beam is evaluated with the Bassetti–Erskine formula and applied to the ions;
  - Ion density and ion-induced E-field is calculated and applied to beam macro-particles.

Although the obtained simulation results showed certain dependence of the growth rate on the initial conditions of the beam, the calculated growth rates agreed well with the predicted asymptotic growth rates. Some of the typical simulation results taken from Ref. [26] are shown in Fig. 14.

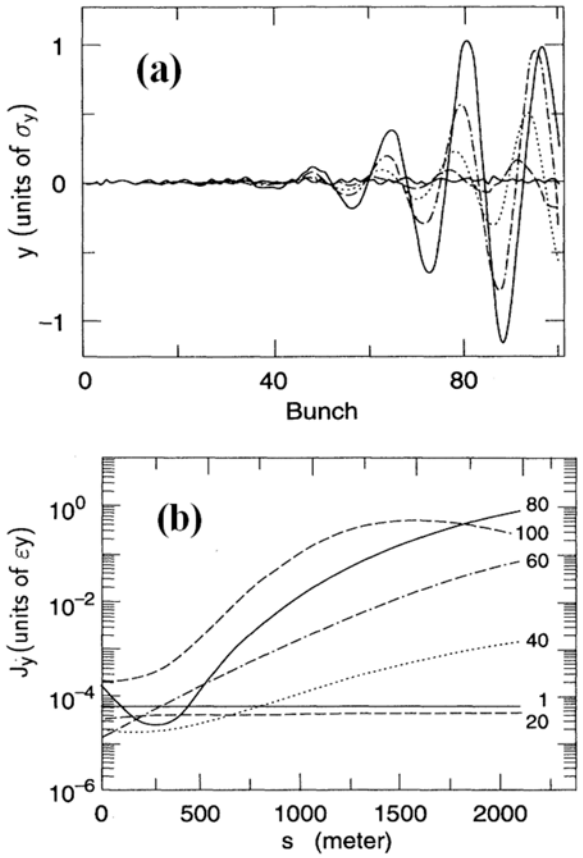

Fig. 14: (a) Growing transverse amplitude of different bunches in a bunch train at several instants. (b) Growth of the transverse action variable J_y versus s (time) for several bunches in a bunch train. Taken from Ref. [26].

Macro-particle simulations of FBII can generally be quite time consuming, especially as the physical process of the collisional ionization is intrinsically sequential and cannot be parallelized. If the bunch distribution of the electron beam can be assumed to not change through its interactions with ions, the beam bunch can be treated as a rigid object (i.e. one macro-particle). Such a model, conventionally called the weak–strong model, can bring about a great simplification and reduction in CPU time [27]. It allows the integration of other physically important ingredients into the simulation, such as transverse bunch-by-bunch feedback and/or the effect of coupling impedance of a ring [28]. The impact of transverse feedback fighting against FBII to stabilize an electron beam is simulated in Fig. 15 using a weak–strong code developed by Xia *et al*. [29].

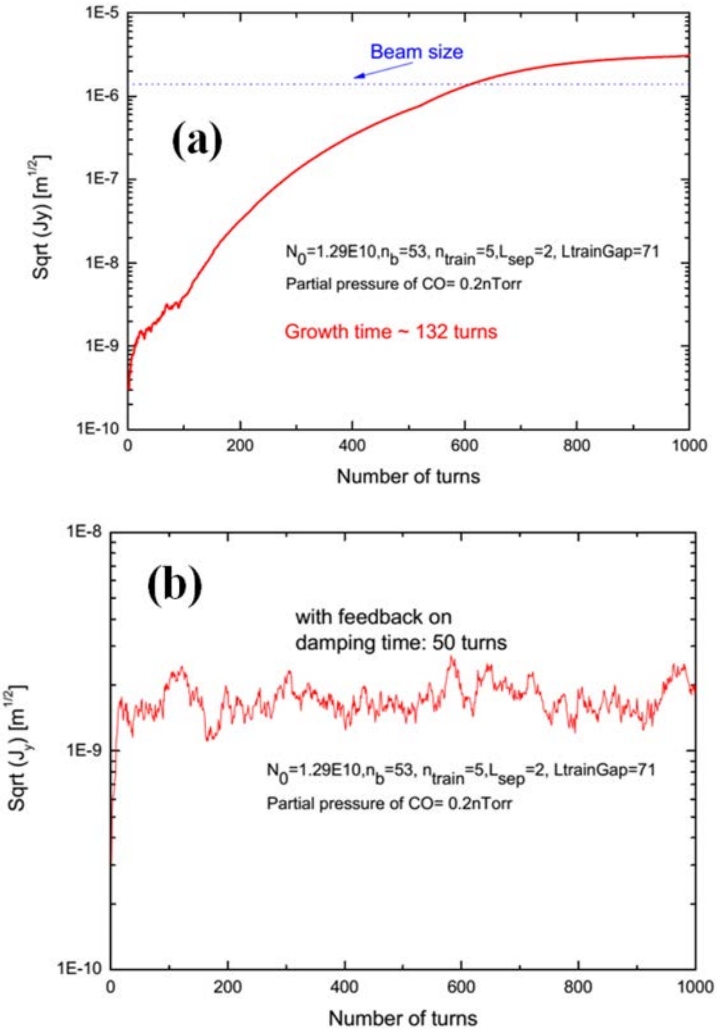

Fig. 15: Simulation of transverse amplitude growth (square root of the transverse action variable J_y) versus time (turn number) without (a) and with (b) bunch-by-bunch transverse feedback. Taken from Ref. [29].

3.2.3 Experimental studies of fast beam–ion instability

The phenomenon of FBII was experimentally demonstrated in ALS [30], PLS [31], and KEK [32] by artificially increasing the vacuum pressure in a ring. Let us follow the major outcomes from the first such attempt made at ALS [30]. As basic conditions, He gas was injected into the ring to increase the vacuum pressure to attain 80×10^{-9} Torr and bunch-by-bunch transverse feedback was switched on to stabilize beam against conventional beam instability such as that due to coupling impedance. A comparison of the vertical beam size was then made to the nominal pressure case as a function of the length of a bunch train, leaving always a large beam gap of more than 80 buckets. A steady increase of

the vertical beam size was observed until the bunch train reached some 15 bunches and then saturated above (Fig. 16). The evolution of the coherent signals exhibited by the beam was followed as a function of its intensity, where the measured peak frequencies turned out to well reproduce what was expected from the theory (Fig. 17). Another interesting observation was the beam current distribution along the bunch train after inserting a vertical scraper to scrape off a vertically blown-up beam (Fig. 18). As expected from the theory, the intensity tended to decrease from the head to the tail of a bunch train. All of these observations well confirmed the characteristics of FBII. Studies made at PLS and KEK gave equally good agreement with theory.

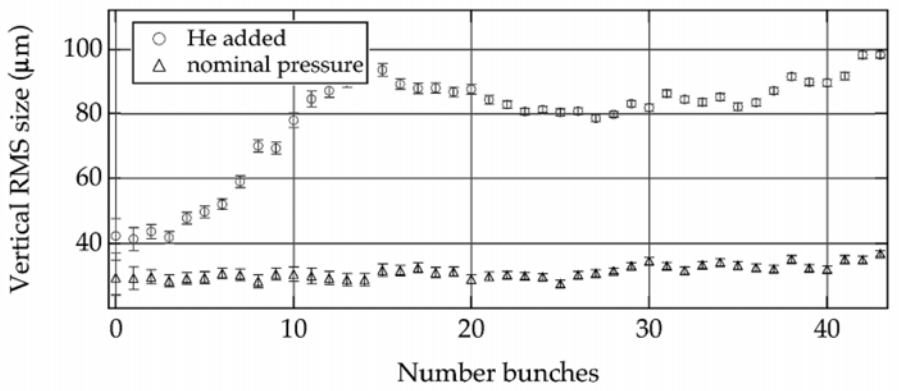

Fig. 16: Measured vertical beam size as a function of the length of a bunch train for two different values of vacuum pressure. Taken from Ref. [30].

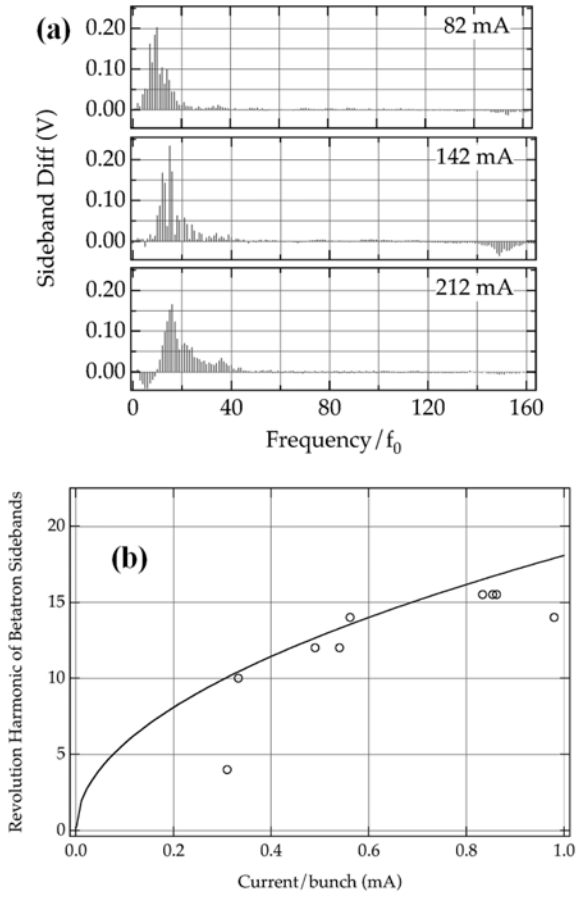

Fig. 17: (a) Measured spectra of coherent vertical beam oscillations at three different beam intensities. (b) Comparison of measured coherent frequencies of beam oscillations with theory. Taken from Ref. [30].

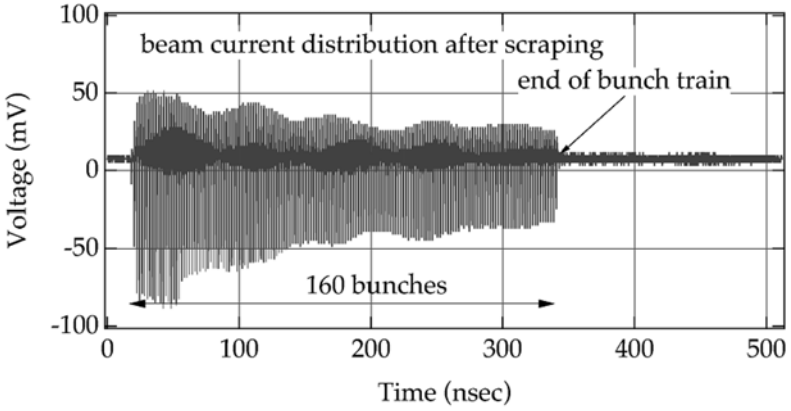

Fig. 18: Measured vertical amplitude along the bunch train after insertion of a vertical scraper. Taken from Ref. [30].

3.2.4 Effect of ion decoherence in growth rate evaluation

In the rest of this section (Subsections 3.2.4 and 3.2.5), let us look at some further theoretical efforts made by several groups to better describe FBII. One that we are going to see here is the influence of ion frequency spread, which exists in reality, but was ignored in the linear model introduced in Subsection 3.2.1. As is known, a spread in the frequency generally helps to reduce the instability growth rate via Landau damping. There are at least three sources of ion frequency spread.

i) Due to the electron beam density variation that may arise from relative transverse displacement of the two beams. As can be seen from Eq. (34), the ion frequency depends on the square root of the electron beam density. So if the transverse extension of an electron beam was finite, as usually represented with a Gaussian distribution, the density of electrons varies according to where an ion probes it.

ii) Amplitude-dependent frequency shift due to the nonlinearity of the static potential of the electron beam.

iii) Electron beam size variations along the ring arising from beta function changes. Again, the dependence of the ion frequency on beta functions can be confirmed from Eq. (34).

To elucidate the effect of ion decoherence analytically, Stupakov *et al*. [33] introduced a distribution function $f(\omega_i)$ on the ion frequency in the previous linear model that we saw in Subsection 1.2.1, and used it to average over all possible transverse ion slices to get the ion beam centroid $y_i(s,t)$ in Eq. (38), with the normalization

$$\int f(\omega_i)\mathrm{d}\omega_i \;=\; 1\ . \tag{42}$$

Proceeding in an analogous way to solve the coupled linear equations as in the earlier model (cf. Eqs. 36 and 37), we arrive at the following equation for the electron beam centroid $y_b(s,z)$:

$$\frac{\partial^2 y_b(s,z)}{\partial s^2} \;+\; \frac{\omega_\beta^2}{c^2}\cdot y_b(s,z) \;=\; -\frac{K}{2z_0}\int_0^z z'\ \frac{\partial y_b(s,z')}{\partial z'}\ D(z-z')\ \mathrm{d}z'\ , \tag{43}$$

where $D(z-z')$ is named as a decoherence function given by

$$D(z-z') \;=\; \int \mathrm{d}\omega_\mathrm{i} \cdot \cos[\frac{\omega_\mathrm{i}}{c}(z-z')] \cdot f(\omega_\mathrm{i}) \;. \tag{44}$$

The physical picture taken here is that the beam–ion instability develops on a time scale that is much larger than both the betatron and ion oscillation periods ($K \ll \omega_\beta^2,\ \omega_\mathrm{i}^2$), which is true in most cases. The above justifies looking for a solution in the form

$$y_\mathrm{b}(s,z) \;=\; A(s,z) \cdot \mathrm{e}^{-\mathrm{i}\omega_\beta s/c + \mathrm{i}\omega_{\mathrm{i}0} z/c} \;, \tag{45}$$

where $\omega_{\mathrm{i}0}$ is the central ion frequency. In the absence of frequency spread $f(\omega_\mathrm{i}) = \delta(\omega_\mathrm{i} - \omega_{\mathrm{i}0})$, the decoherence function becomes unity and the solution $A(s,z)$ is confirmed to consistently reduce to the asymptotic solution found in Subsection 1.2.1. In Ref. [33], the decoherence functions in the exponential form were explored to be able to derive analytically the solutions $A(s,z)$ for the first two sources of the frequency spread given above. Analytical results were found to be in good agreement with macro-particle simulations, where the treated ion tune spreads caused a reduction of the instability growth rate by roughly a factor of 2.

3.2.5 Wake function description of an ion cloud

The second theoretical development we shall look at is about modelling a fast beam–ion interaction with a transverse dipolar wake function or, equivalently, the machine-coupling impedance that is its Fourier transform, conventionally used to describe the interaction of a beam with its surrounding vacuum chambers. A first such attempt was in fact made in describing a positron coasting beam driven unstable by an electron cloud [34]. An analogous treatment extending the idea to ion clouds interacting with bunched electron beam was then made by two groups [22, 35]. Here let us briefly follow the work of Wang *et al*. in Ref. [22]. There is initially an ion cloud formed by collisions of electrons with residual gases, consisting on N_i ions. If there then comes an electron bunch composed of N_e electrons with its centre of mass deviated by $\Delta y_{\mathrm{e}0}$ from the centre of the ion distribution, assumed to be described with a Gaussian, the ion distribution gets a kick from the electron bunch and starts oscillating coherently. The oscillating ion distribution can in turn give a kick $\Delta\overline{y}_\mathrm{e}'(s)$ to another electron bunch following the first bunch at a distance s behind. If the initial displacement $\Delta y_{\mathrm{e}0}$ is small enough and corresponds to the linear part of the ion distribution, all of this process can be followed analytically using the relations derived in previous sections. In addition, we find that $\Delta\overline{y}_\mathrm{e}'(s)$ is proportional to $\Delta y_{\mathrm{e}0}$ so that the transverse dipolar wake excited by a bunch of electrons is defined by

$$W_y(s) \;\equiv\; \frac{\gamma}{N_\mathrm{e}\varepsilon_0 r_\mathrm{e}} \cdot \frac{\Delta\overline{y}_\mathrm{e}'(s)}{\Delta y_\mathrm{e}} \;\; [\mathrm{V C^{-1}\, m^{-1}}], \tag{46}$$

which does not depend on $\Delta y_{\mathrm{e}0}$, namely it satisfies the linear response condition. The linearity of the wake function $W_y(s)$ as defined above was numerically confirmed, as shown in Fig. 19, where the wakes excited by various values of $\Delta y_{\mathrm{e}0}$ are seen to converge on the same values.

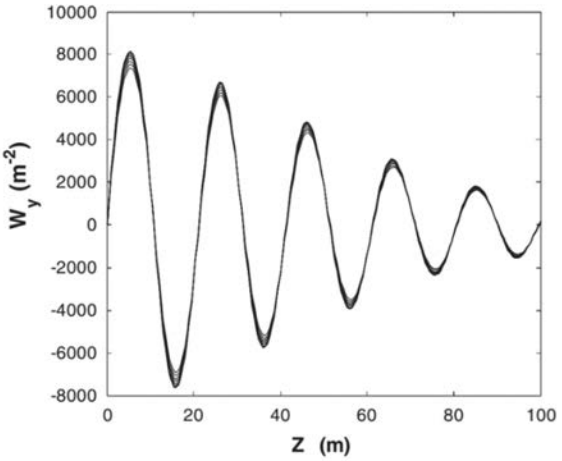

Fig. 19: Simulated wakes of an ion cloud for various Δy_{e0} ranging from one tenth to one sigma with a step of one tenth of a sigma. Taken from Ref. [22].

Also noticed for $W_y(s)$ (Fig. 19) is the damping of the oscillation, which is due to the nonlinearity of the beam–ion space charge force, inducing an ion frequency spread. Wang *et al*. managed to parameterize the wake function in the usual broadband resonator function as

$$W_y(s) \;=\; \hat{W}_y \cdot \exp\{-\omega_i s/(2Qc)\} \cdot \sin\left(\frac{\omega_i s}{c}\right) \tag{47}$$

where

$$\hat{W}_y \;=\; \frac{N_i}{\varepsilon_0}\left(\frac{r_p L_{sep}}{A N_e}\right)^{1/2} \cdot \left[\frac{4}{3}\cdot\frac{1}{\sigma_y(\sigma_x+\sigma_y)}\right]^{3/2} \;[\mathrm{VC^{-1}m^{-1}}], \tag{48}$$

and the Q values close to 9 were found to reproduce well the numerically obtained wakes of most of the ions and electron beam sizes (Fig. 19). The impedance function corresponding to $W_y(s)$ in Eq. (47) is therefore given by

$$Z_y(\omega) = \frac{\hat{W}_y}{\omega}\cdot\kappa\cdot\frac{Q}{1 + \mathrm{i}Q\left(\frac{\omega_i}{\omega}\frac{1}{\kappa} - \frac{\omega}{\omega_i}\kappa\right)} \;\approx\; \frac{\hat{W}_y}{\omega}\cdot\frac{Q}{1 + iQ\left(\frac{\omega_i}{\omega} - \frac{\omega}{\omega_i}\right)}\,, \tag{49}$$

where $\kappa = \sqrt{1-1/(2Q)^2} \approx 1$.

The advantage of describing the beam–ion dynamics of a wake or an impedance function is to be able to use the same linearized Vlasov equation formalism developed for conventional coupled-bunch instabilities. In Ref. [22], an application was made to study the stabilization effect of beam gaps introduced in a bunch train.

4 Mitigations and observations of ion effects

In the first part of this section, we shall briefly review various mitigation techniques developed and applied in the past against ions. Three examples of experimental studies of beam ion instabilities shall

then be introduced. The first example is about ion trapping at the Photon Factory (KEK), and the two others are on FBII (SPEAR3 and SOLEIL).

4.1 Mitigations of ion effects

4.1.1 Partial beam fillings/multi-bunch trains/bunch gaps

Partial beam fillings have long been known to be one of the most efficient methods for avoiding ion trapping, and have been constantly applied in the storage rings of today [10, 14, 36]. One can intuitively understand that, during a beam gap, ions see no electrostatic potential of the beam and therefore they can drift away. Numerically, this would correspond to not finding a stable linear solution in the transfer matrix approach explained in Section 2.9 in working with an extended one-turn matrix that integrates a drift matrix that represents the beam gap [37].

As already mentioned, FBII may arise even in the presence of a large beam gap since ions could be generated during a single passage of a bunch train and strongly interact with it in a resonant manner from turn to turn. In such a case, cutting a long bunch train into small pieces and introducing small bunch gaps between the short trains generally helps to reduce the FBII growth rate. Such a study was made by Wang *et al* using the wake function formalism explained in Subsection 3.2.5 (Fig. 20) [22]. An exception to this physical picture has been observed at SOLEIL where, contrarily, partial fills enhance FBII. We shall see this phenomenon in more detail in Subsection 4.2.3.

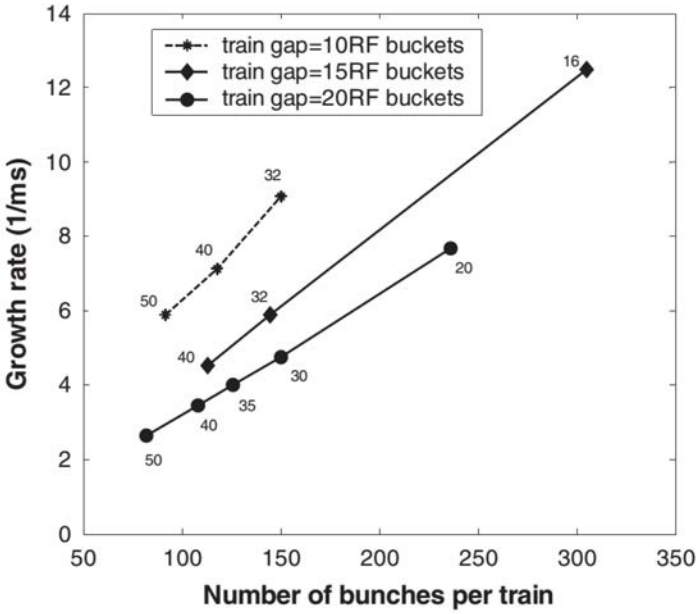

Fig. 20: Calculated growth rate of FBII for different beam fillings, as a function of the number of bunches per bunch train. Three different train gaps of 10, 15, and 20 buckets are considered. The number of bunch trains is also shown in the plot. Taken from Ref. [22].

4.1.2 Ion-clearing electrodes

Introducing a pair of electrodes as shown in Fig. 21 to clear the trapped ions away is also a method known to be effective in reducing ion effects [13, 16, 37]. This worked successfully in several rings such as SRS (Daresbury) [38], ISR (CERN) and Aladdin (University of Wisconsin) [39]. As we saw in Section 2.5, it is efficient to install the electrodes where the beam potential is at a local minimum so that the ions drift and are gathered. To expel ions, the voltage on the electrodes needs be higher than the electrostatic potential of the beam, which for electron beams is typically in the hundreds of volts range (cf. Fig. 3), while for proton beams, it can reach a range of some kilovolts. A too-high voltage may increase the risk of bombarding the accelerated ions on the chamber walls, which in turn could induce

outgassing as observed in proton rings [7, 17]. Ion-clearing electrodes have the disadvantage of increasing the broadband impedance of a ring, decreasing the single-bunch instability thresholds or inducing local machine heating. Optimization of the electrode design should be done in advance to minimize the impedance [40].

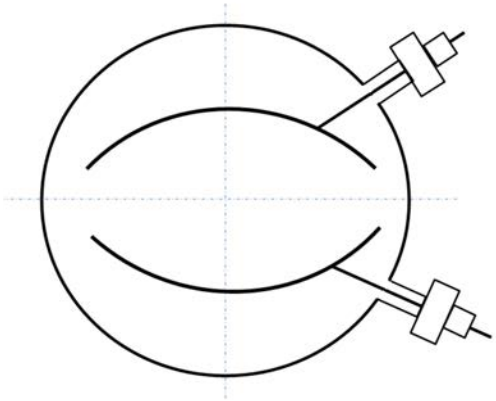

Fig. 21: An illustration of ion clearing electrodes

4.1.3 Positron beam storage

In a ring where a stored electron beam is under the influence of trapped ions, replacing it with a positron beam should resolve the problem of ion trapping, as the positron beam will not attract the ions, which have the same positive charge. In addition, if we recall the discussions of the critical mass in Section 2.9, electrons, which have the opposite charge, are not likely to be trapped by the positron beam since the electron mass is so small. For this reason, a number of lepton storage rings, such as DCI, ACO, SUPERACO, Photon Factory, APS and PETRA-III [15, 41–43], have operated quite successfully with positron beams. However, when the intensity of a stored beam gets high, an electron cloud may be formed via synchrotron radiation generating photo-electrons and lead to electron-cloud instability. Historically, the electron-cloud instability was identified at Photon Factory (KEK) as one of the earliest observations upon changing the stored beam from electrons to positrons to avoid ion trapping [44].

4.1.4 Use of octupoles/chromaticity shifting

Octupole and sextupole magnets can create betatron tune spreads in an electron beam either via an on-momentum amplitude-dependent tune shift or by an off-momentum tune shift with non-zero chromaticity, which can Landau damp ion instability. At Photon Factory (KEK), the combination of the use of octupoles and a partial fill, as explained above, managed to completely suppress ion instability [18]. Since these nonlinear elements simultaneously reduce the dynamic acceptance of a ring in general, however, one needs to evaluate in advance optimal strengths for these elements.

4.1.5 Radio-frequency knockout

Shaking a beam that is under the influence of trapped ions with an external RF field may have the effect of chasing the ions away. Such attempts were made at UVSOR and Photon Factory where the beams were shaken with frequencies in the megahertz range [12, 13]. However, shaking a stored beam may not be an optimal solution in light sources in which excellent beam stability is usually required.

4.1.6 Transverse bunch-by-bunch feedback

With the performance of feedback systems available on the market today, this would be the best method to stabilize a beam against ion instability, whether it is due to ion trapping or FBII. As long as the two-beam instability concerns interaction between the centres of mass as we have described in Section 3, and that the instability growth rate does not exceed the feedback damping time, which appears to be true

in most cases, transverse bunch-by-bunch feedback should be able to stabilize each bunch separately. Experience gained at ESRF and SOLEIL confirm this feature [45, 46]. In both rings, the ion frequencies are typically in the range of a few tens of megahertz, which is low compared to the feedback bandwidth of 176 MHz for these machines. The beam oscillations can therefore be corrected relatively easily. An example is shown in Fig. 22. For future accelerators, however, higher feedback performance may be required to fight against FBII with extremely short growth times. Again at SOLEIL, an exceptional case of feedback turning out to be destructive under extreme situations has been observed, which will be described in more detail in Subsection 4.2.3.

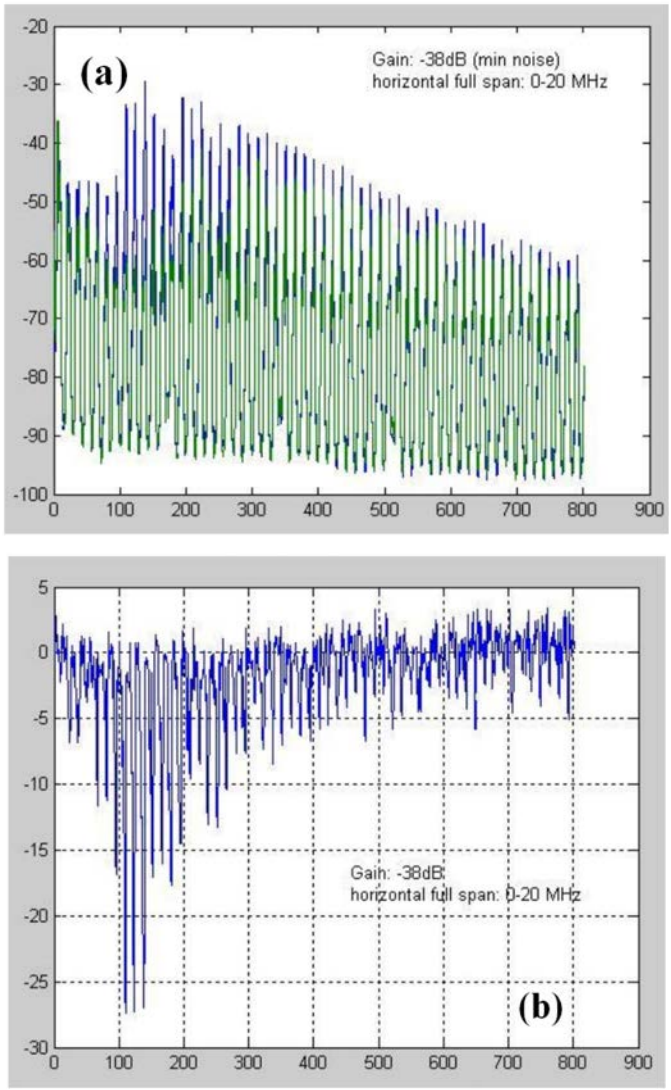

Fig. 22: Vertical beam spectra with (green) and without (blue) transverse bunch-by-bunch feedback in the uniform filling measured at the ESRF. (a) Total amplitude. (b) Difference in amplitude between the two cases. Horizontal axis spans 0-20 MHz. Taken from Ref. [45].

4.1.7 Reduced vertical beam size (by more than a factor of two)

Through theoretical studies of FBII, an interesting idea has emerged that if an electron beam can only blow-up vertically by roughly a factor of two and never get lost due to saturation of the two-beam interaction, one may reduce the vertical beam size by a factor of two in advance by taking blow-up into account [47]. More studies may be needed to fully certify the absence of residual beam blow-up in the saturation regime before employing such a scheme.

4.1.8 Enhancing vertical beta function variations

As we saw in Subsection 3.2.1, the absence of FBII in many modern light sources suggests sources of stabilization in these machines, among which the strong variations of beta function are suspected as they induce ion frequency spreads. Going further along this direction, we may actively enhance vertical beta function variation to stabilize the beam via Landau damping. Again, more numerical studies may be required to certify the damping mechanism quantitatively.

4.2 Observations of ion effects

4.2.1 Experimental characterizations of ion trapping at Photon Factory

A unique and interesting set of measurement have been made at Photon Factory (KEK) that elucidate in more detail the dynamics of the two-beam instability induced by trapped ions. We have already seen in Fig. 9 (Section 2.1) that the instability gives rise to a pulsation of the stored beam with a frequency in a range of some tens of hertz, which is, in fact, particularly disturbing to synchrotron light users. First, the dependence of the pulsation frequency on the vacuum pressure was investigated by controlling the number of Distributed Ion Pumps (DIPs) activated (Fig. 23). A clear trend can be seen in which the frequency elevates as the vacuum pressure gets higher [48].

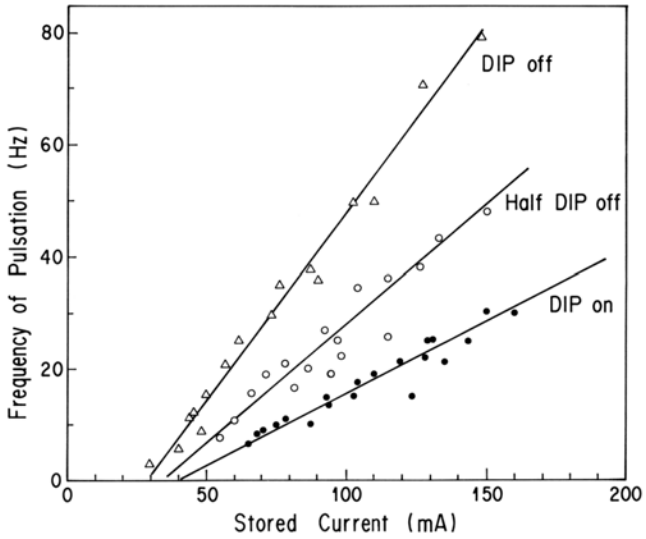

Fig. 23: Dependence of the measured frequencies of the vertical beam pulsation on beam intensity and vacuum pressure. Taken from Ref. [18].

To have a deeper insight into the cycle of pulsation, the bremsstrahlung count rate was followed for the different conditions of the vacuum pressure above [49, 50]. We note here that when there are trapped ions, circulating electrons collide with the nuclei of ions and produce γ rays. Relative changes of the count rate in time would reflect the variation of ions at a local point in the ring, as a change in the vertical size of an electron beam itself would not alter the collision rate with residual gases. The time evolution of the count rate was measured under two different conditions (Fig. 24): both the vacuum pressure and the beam current are lower in Fig. 24(a) than in Fig. 24(b). In Fig. 24(a) we can observe two slopes for the count rate, namely one that corresponds to when the blown-up electron beam is radiation damping and attracting more ions; and another where a slower increase of ions after the electron beam has converged to its original size. The second process is supposed to continue until an instability threshold in the ion density is reached. In Fig. 24(b), on the other hand, we cannot distinguish the two slopes, and the instability threshold is seemingly reached rapidly during the process of radiation damping.

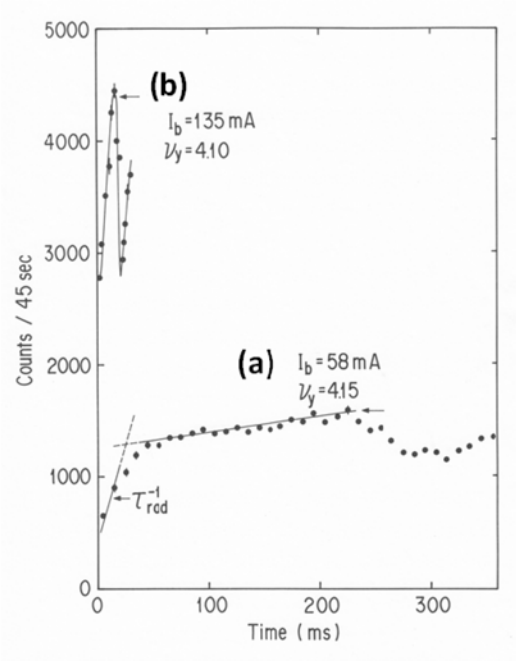

Fig. 24: Time evolution of the Bremsstrahlung count rate measured at two different beam intensities. See text for the different experimental conditions employed for (a) and (b). Taken from Ref. [18].

The bremsstrahlung count rate was compared between the uniform and a (2/3-like) partial filling under the same vacuum condition and the beam current (Fig. 25). The clearly higher rate observed for the uniform filling should signify a larger number of ions trapped in this filling mode.

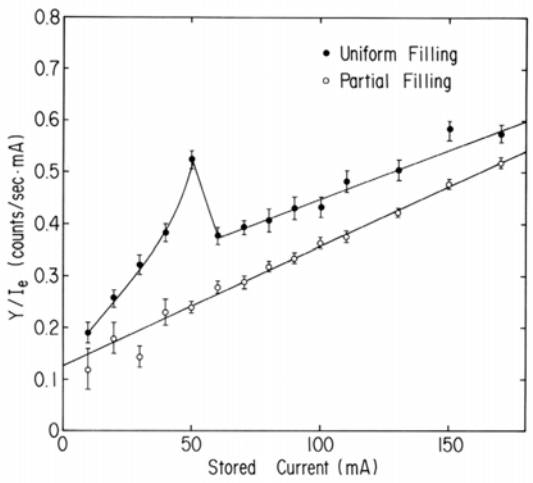

Fig. 25: Measured Bremsstrahlung count rate versus beam intensity for two different beam fillings. Taken from Ref. [18].

4.2.2 Experimental characterizations of fast beam–ion instability at SPEAR3

A systematic characterization of FBII was made at SPEAR3 (SLAC) by measuring the vertical betatron sideband signals over the multi-bunch frequency band under different beam and machine conditions [51]. In their work, these experimental results are also compared with those expected from theory using the wake formalism explained in Subsection 3.2.5. Three such sets of measurement are cited here. The first one concerns the dependence on the vertical beam size, which is adjusted with skew quadrupoles. Without them, the beam size is about 2.3 times larger. As we expect from theory (cf. Eqs. (32–34)), the two-beam interaction gets significantly enhanced as the beam size is reduced (Fig. 26).

The dependence on the bunch filling pattern is shown in Fig. 27. In all three cases shown, the total number of bunches (= 280), the bunch gap (= 15 buckets) and the total beam current (= 500 mA) are kept equal. The comparison clearly indicates the advantage of filling a beam in many short trains of bunches in fighting against FBII. The third measurement concerns the dependence on the vertical chromaticity, which is increased from 2 to 7 (Fig. 28). Again, as expected the chromaticity helps suppression of FBII, presumably through an increased tune spread of the electron beam, though it is clearly correlated with lifetime reductions as indicated in the figure.

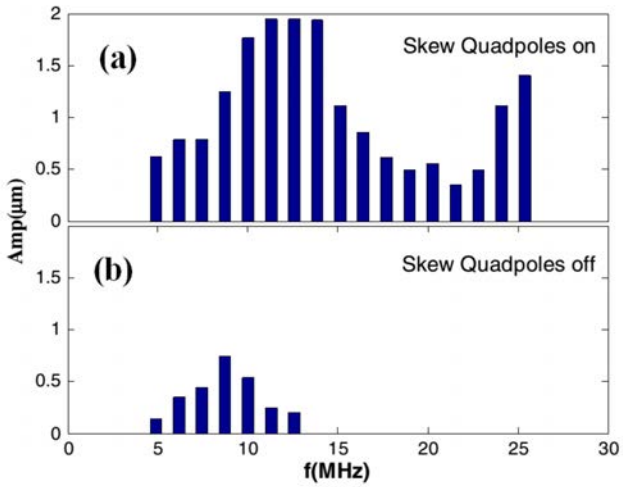

Fig. 26: Measured vertical beam sizes of a single bunch-train (280 bunches) at 192 mA with (a) and without (b) skew quadrupoles. When skew quads were switched off (b), the vertical beam size became roughly 2~3 times larger. Taken from Ref. [51].

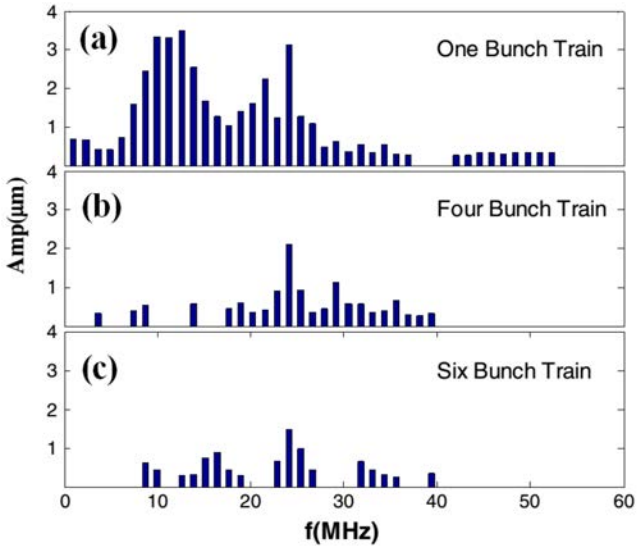

Fig. 27: Measured vertical amplitudes of a stored beam for different fillings. In all cases, there are 280 bunches and the total current is 500 mA. The bunch train gap is 15 buckets (32 ns). Taken from Ref. [51].

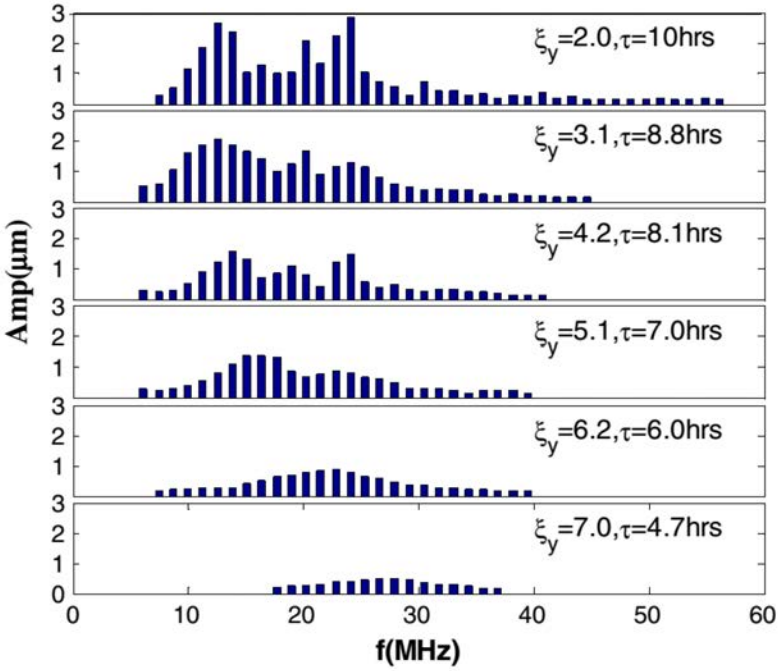

Fig. 28: Measured vertical amplitudes of a stored beam versus vertical chromaticity. Single bunch-train (280 bunches) at 500 mA. Horizontal chromaticity is kept at 2. Taken from Ref. [51].

4.2.3 Beam losses due to a combined effect of fast beam–ion instability driven by beam-induced outgassing, resistive-wall instability, and transverse feedback at SOLEIL

We shall describe below the beam losses, which are often total losses, encountered at SOLEIL at high beam current. After a series of experimental and numerical investigations, these losses were identified as being due to FBII that induces a somewhat complicated combined effect involving Resistive-Wall instability (RW) and transverse feedback [46, 52]. A noteworthy associated feature is that the FBII does not arise from the ordinary vacuum pressure, but occurs uniquely due to localized outgassing of vacuum chambers that are heated by the circulating beam via wake fields.

The fact that multi-bunch operation at SOLEIL is under the influence of a mixture of resistive-wall and ion instabilities was known since the time of commissioning through the analysis of data available from the bunch-by-bunch transverse feedback diagnostics. Transverse feedback was switched off over a short period of time (usually around 1 ms) to let the beam blow up, and the bunch-by-bunch data were acquired over this period of time. The results typically showed that at relatively low current, the beam is under the influence of RW, as seen from the amplitude and phase relations in a bunch train (Figs. 29(a) and 29(b)). However, above a certain current, which is roughly 100 mA in Fig. 29, there is a transition to FBII. In particular, both the bunch-to-bunch betatron phase variations of ~0.9° and ~40° measured (Fig. 29(b)) are in good agreement with what expected from RW and FBII instabilities, respectively. The measured growth rate versus current, averaged over bunches, follows well the curve expected from the RW instability, but with larger error bars at high current, suggesting the nature of mixture of the two instabilities (Fig. 30).

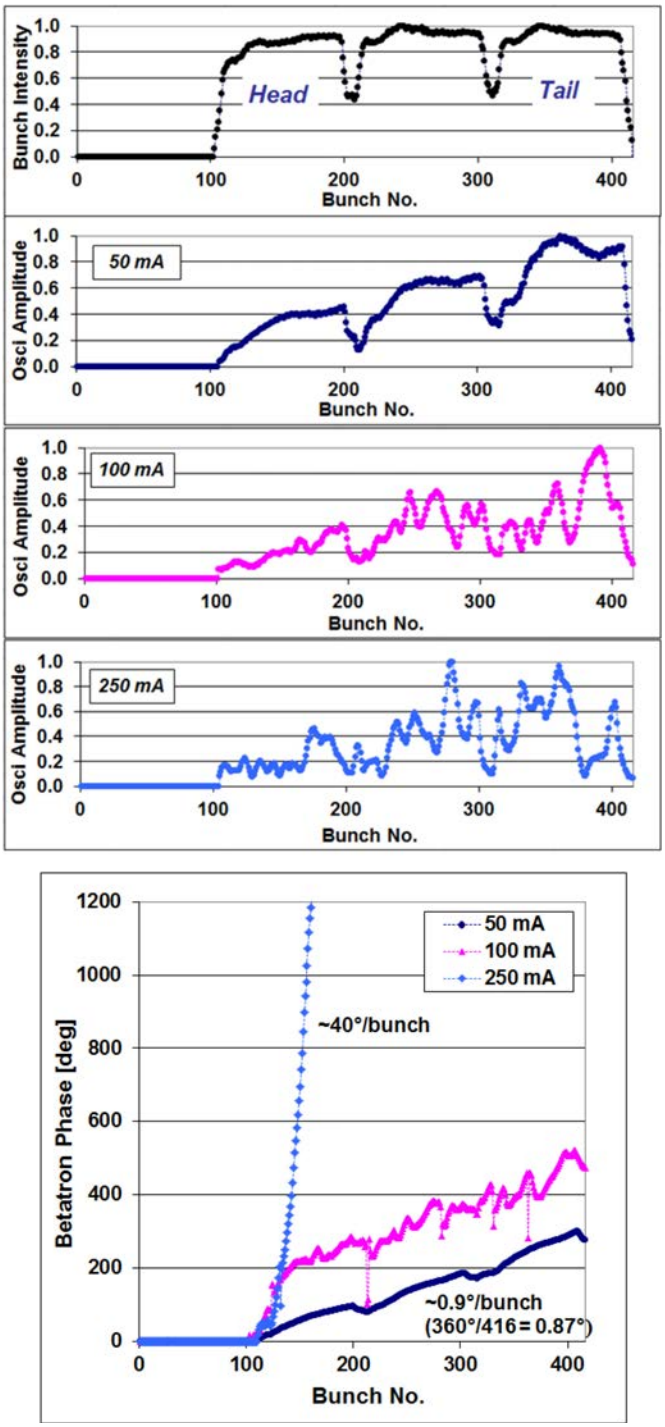

Fig. 29: (a) Vertical amplitude versus bunches in ¾ filling measured as a function of beam current. (b) Measured relative betatron phase with respect to adjacent bunches in a bunch train in correspondence to the cases in (a). Taken from Ref. [53].

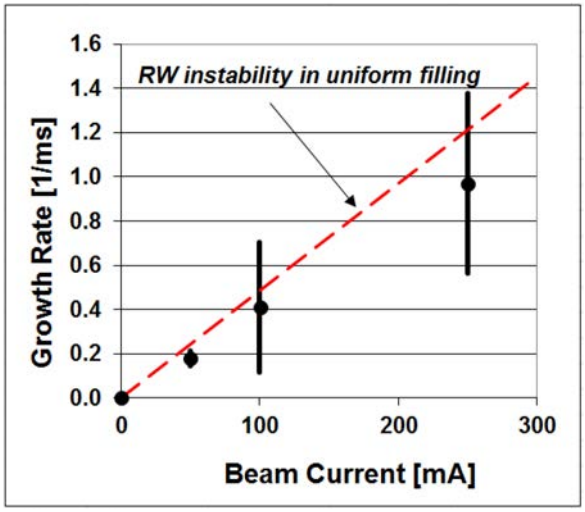

Fig. 30: Growth rate of vertical instability as a function of beam current measured corresponding to the cases in Figs. 29 [53].

Although vacuum conditioning with beam over the years helped to reduce the relative contributions of FBII at a given beam current, as confirmed by re-performing the measurement as described above, FBII still persistently exists at SOLEIL at the nominal current of 500 mA, after nearly 10 years of operation. As already mentioned it often causes beam losses, which strangely happen some ten minutes after ramping the current to its final value. During this period, the beam is diagnosed as being stable. To avoid the beam losses, a number of different beam fillings were tried under the assumption that beam gaps are effective against FBII. However, the experimental results indicated that, to the contrary, the uniform filling gives the most stable beam. This, along with the finding that reducing the RF voltage greatly helps increasing the beam stability, led one to realize that the source of FBII is the beam-induced heating of vacuum chambers via longitudinal wake fields, which in turn triggers outgassing. Thus, keeping the bunch current low and the bunch length long to avoid heating becomes of primary importance. Also, the beam losses were understood to be due to the machine interlock that trips the RF upon detecting a rapid drop of beam current to protect the RF system.

It remained to be understood why the beam current suddenly drops so as to trigger a machine interlock. Once again, the bunch-by-bunch diagnostics, used for a post mortem, helped to get a closer look into what happens to the beam in the last moment before it gets lost (Fig. 31). In Fig. 31(a) where the averaged amplitude of the beam is plotted against time, we see that the beam blows up exponentially before it is lost. This suggests that the sudden current drop is due to the blown-up beam being scraped off either by the vacuum chamber or by the dynamic acceptance. Analyzing the phase relation between adjacent bunches as done in Fig. 29(b) above, we can identify chronologically the appearance of the following three regimes up to the explosion: Fig. 31(b) no phase correlation (i.e. absence of coherence); Fig. 31(c) ion regime; and Fig. 31(d) RW regime. We see in Fig. 29(a) that for some reason transverse feedback fails to keep the beam stable when it is in the ion regime.

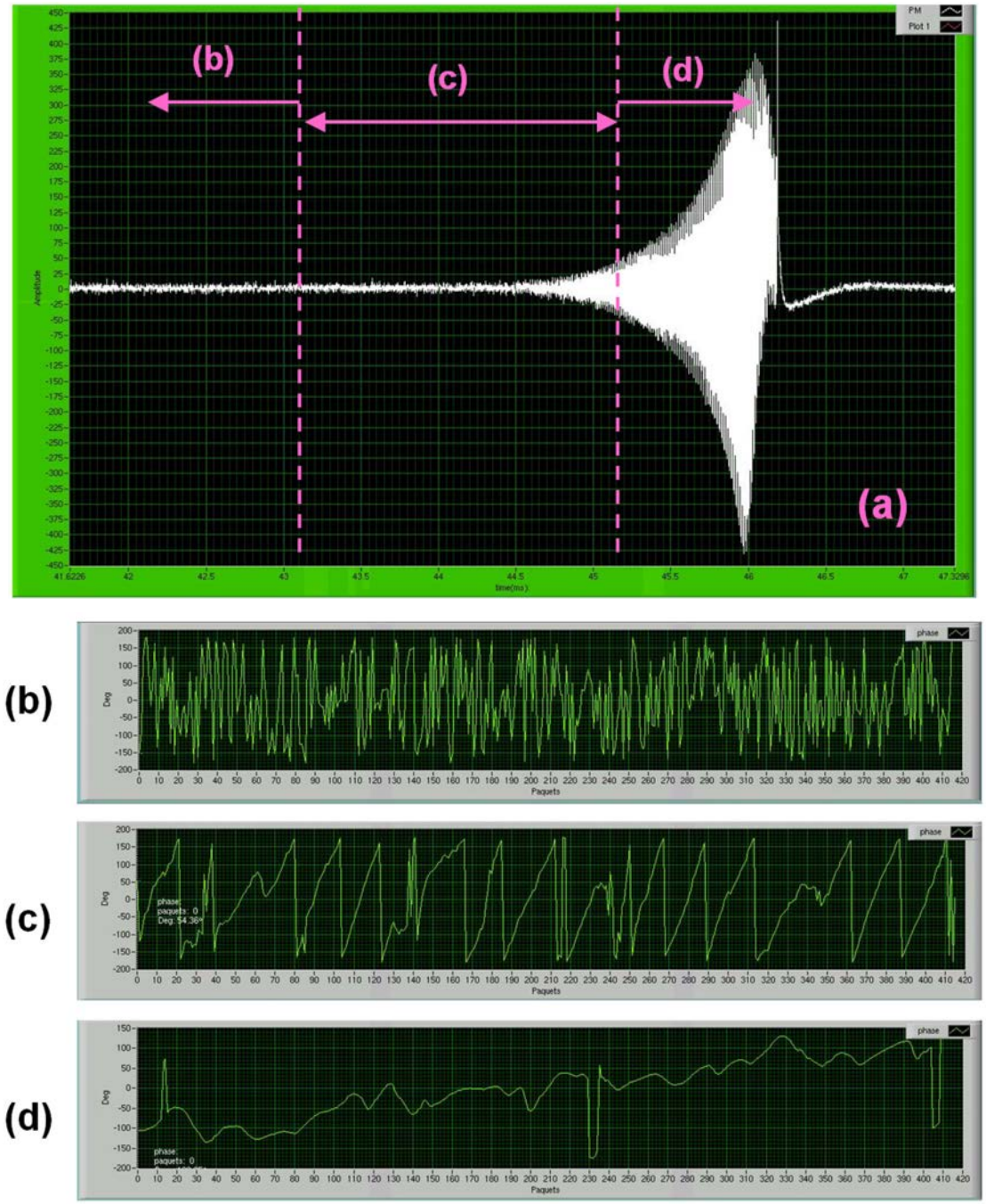

Fig. 31: (a) Measured evolution of the vertical oscillation amplitude average over bunches in ¾ filling versus time. The beam blows up and gets lost at around 46 ms after the beginning of the measurement. Measured relative betatron phase with respect to adjacent bunches along the bunch train identifies three different regimes differentiated in time as indicated in Fig. 31(a): (b) no phase correlation; (c) ion regime; (d) RW regime.

The last observation implies that during some ten minutes of 'silence', the gas density, and therefore the number of ions created at each turn, steadily increase up to the point that the FBII growth rate exceeds the limit of feedback, since the underlying machine heating continues. What is not obvious, however, is the reason why the beam continues to blow up in the RW regime when ions would probably be gone due to large beam oscillations. Namely, we need to understand the failure of feedback in the third RW regime. A possible explanation is that feedback, with its filter and gain used, is not reacting well enough against the fast dynamical change of the beam from FBII to RW. More details are found in

Ref. [53]. A simulation study that includes the effects of RW, FBII, and feedback reproduces the beam behaviour in a similar manner to that observed, supporting the above conjecture (Fig. 32).

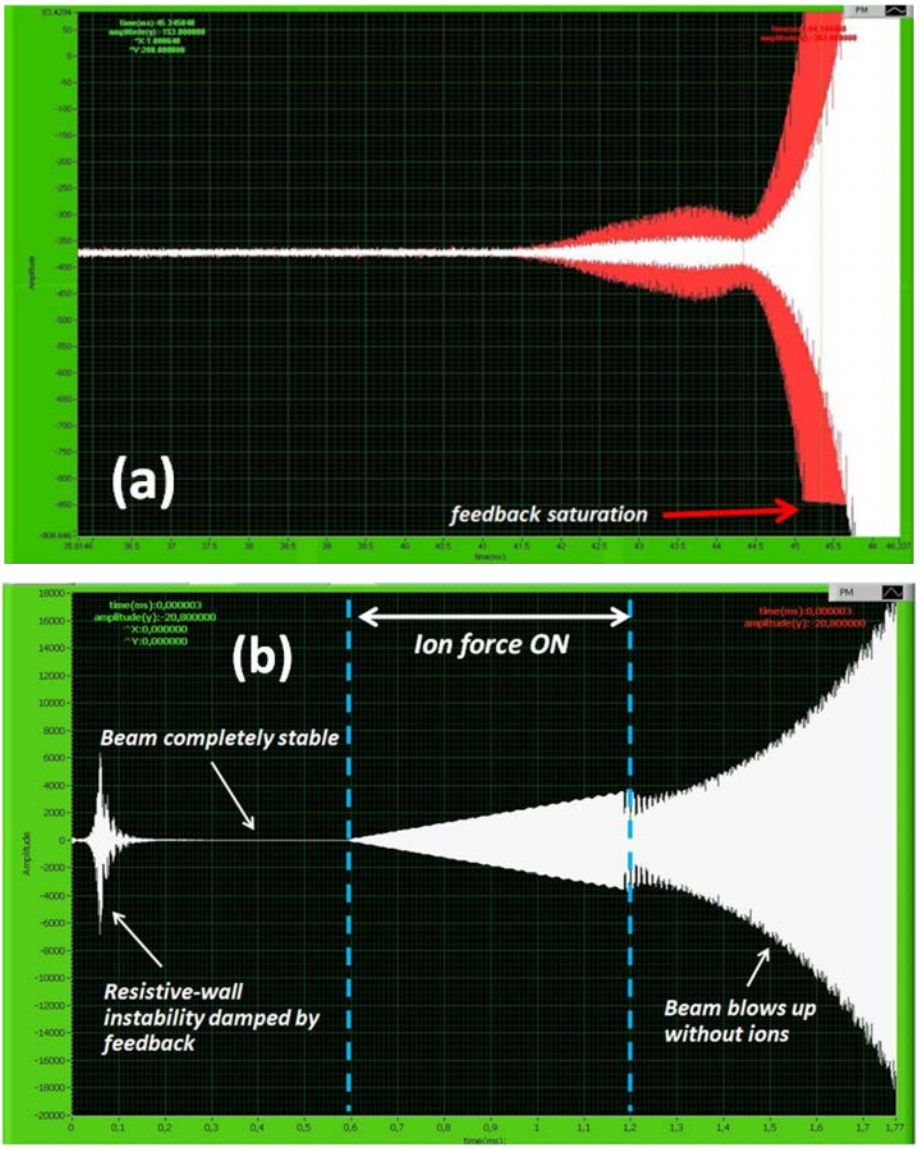

Fig. 32: (a) Measured evolution of the vertical oscillation amplitude (in white) average over bunches in ¾ filling versus time. The beam blows up and gets lost at around 46 ms after the beginning of the measurement. Amplitude of kicks given by bunch-by-bunch feedback is superimposed in red. (b) Simulation of FBII including the resistive-wall (RW) instability and bunch-by-bunch feedback. The beam blows up after the ions have disappeared in the regime feedback works against RW instability. Taken from Ref. [53].

5 Conclusions

Due to the general difficulties of measurement and frequent non-reproducibility of vacuum conditions, beam instabilities arising from ions in the beam duct are often not straightforward to understand, as compared to other collective instabilities. However, the theoretical, numerical, and experimental studies made so far, creating a solid basis for beam–ion physics, allow fairly good explanations and qualitative and quantitative predictions. There are still a number of nonlinear beam–ion dynamics involving Landau damping and stabilization that are not adequately understood, and would require further efforts.

Owing presumably to lower beam emittances in modern storage rings, ion trapping does not seem to be a big issue anymore. However, FBII could jeopardize the performance of future low emittance and high beam intensity accelerators, as its growth rate would get larger. For light sources, in particular, the effort of reaching an ultra-low emittance tends to render the vacuum chamber aperture smaller and smaller. The vacuum issues and hence ion-induced beam instabilities would likely remain important, especially in a combined manner with other effects, as already encountered at SOLEIL. Continuation of beam–ion studies would therefore be of great importance in raising the performance of future accelerators.

Acknowledgements

The author thanks Christian Herbeaux, Nicolas Béchu, Nicolas Baron, the SOLEIL vacuum experts, as well as his colleagues in the accelerator physics group at SOLEIL for useful discussions in preparing this presentation. He thanks Amor Nadji, the Division Head of SOLEIL, for his support of this work. He expresses his special thanks to Shogo Sakanaka at KEK for his helpful remarks, providing the original figures from his studies used in this paper, and for his lecture notes created for the KEK Accelerator School OHO86 (Ref. [18]), from which the present paper much profited.

All figures used in the present paper that are cited from other published papers and notes have their origins explicitly referenced and their copyright permissions properly acquired prior to the publication of this lecture note.

References

[1] R. Jolivot, Anneaux de Stockage. Le piégeage des ions dans ACO et leur balayage, Rapport technique 75-63/RJ-FB, Ecole Normale Supérieur – Faculté des Sciences, Orsay, Laboratoire de l'Accélérateur Linéaire (1963).

[2] B. Angerth, Review of studies on beam neutralization in storage rings, AR/Int. SG/65-1 (1965).

[3] E. Fischer, Clearing fields for the ISR, ISR-VAC/66-15 (1966).

[4] D. Poteaux, Piégeage des ions dans un anneau e^+e^-, Rapport technique 29-69 DP/LN Laboratoire de l'Accélérateur Linéaire, Orsay (1969).

[5] R.D. Kohaupt, Mechanismus der ionenabsangung im Electron Positron Speicherring Doris, Interner Bericht DESY H1-71/2 (1971).

[6] D.G. Koshkarev and P.R. Zenkevich, *Part. Accel.* **3** (1972) 1.

[7] R. Calder, E. Fischer, O. Gröbner and E. Jones, Vacuum conditions for proton storage rings, CERN/ISR-VA/74-26 (1974).

[8] Technical Note – ISR Vacuum Group, The behaviour of ions in presence of a bunched antiproton beam in the ISR, ISR-VA/EF-sm (1978).

[9] Y. Baconnier and G. Brianti, The stability of ions in bunched beam machines, CERN/SPS/80-2 (DI) (1980).

[10] Y. Yamazaki, M. Kihara and H. Kobayakawa, Partially filled multi-bunch mode operation of the Photon Factory electron storage ring and cure of the vertical instability, KEK 83-17 (1983), KEK internal report.

[11] A. Poncet, Ion clearing in EPA, PS/ML/Note 83-1, CERN internal report.

[12] Y. Kamiya, M. Izawa, T. Katsura, M. Kihara, H. Kobayakawa and S. Shibata, Vertical instability caused by ion-trapping in KEK-PF storage ring, Proc. 5th Symp. Acc. Sci. Tech. p. 292. , KEK, Tsukuba, Japan (1984).

[13] T. Kasuga, H. Yonehara, T. Kinoshita and M. Hasumoto, *Jpn. J. Appl. Phys*. **24** (1985) 1212, http://dx.doi.org/10.1143/jjap.24.1212

[14] M.Q. Barton, *Nucl. Instrum. Meth.* **A243** (1986) 278, http://dx.doi.org/10.1016/0168-9002(86)90961-7

[15] H. Kobayakawa, *Part. Accel*. **33** (1990) 81.

[16] G. Brianti, in Proceedings of the CAS-CERN Accelerator School: Antiprotons for Colliding-Beam Facilities, Geneva, Switzerland, 11-21 October 1983, edited by P. Bryant and W.S. Newman, CERN-1984-015 (CERN, Geneva, 1984), pp. 369-383, http://dx.doi.org/10.5170/CERN-1984-015.369

[17] Y. Baconnier, in Proceedings of the CAS-CERN Accelerator School: General Accelerator Physics, v.1, Gif-sur-Yvette, France, 3-14 September 1984, edited by P. Bryant and S. Turner, CERN-1985-019 (CERN, Geneva, 1985), pp. 267-300, http://dx.doi.org/10.5170/CERN-1985-019-V-1.267

[18] S. Sakanaka, Phenomena of ion trapping in storage rings, KEK accelerator school lecture note [in Japanese], OHO'86, KEK, Tsukuba, Japan (1986).

[19] M. Bassetti and G.A. Erskine, Closed expression for the electrical field of a two-dimensional Gaussian charge, CERN-ISR-TH/80-06 (1980).

[20] M.E. Biagini, S. Guiducci, M. Preger, M. Serio and S. Tazzari, Observation of ion trapping at ADONE, Proc. 11th Int. Conf. on High Energy Accelerators, p. 687, CERN, Geneva, Switzerland (1980).

[21] P.F. Tavares, Transverse distribution of ions trapped in an electron beam, CERN-PS/92-55 (LP) (1992).

[22] L. Wang, Y. Cai, T.O. Raubenheimer and H. Fukuma, *Phys. Rev. STAB.* **14** (2011) 084401, http://dx.doi.org/10.1103/physrevstab.14.084401

[23] K.Y. Ng, *Physics of Intensity Dependent Beam Instabilities* (World Scientific, 2005), p. 609, http://dx.doi.org/10.1142/5835, 5 Toh Tuck Link, Singapore 596224

[24] E. Keil and B. Zotter, Landau damping of coupled electron–proton oscillations, CERN-ISR-TH-71-58 (1971).

[25] Coherent instability due to electrons in a coasting proton beam, edited by H. G. Hereward, CERN-1971-015 (CERN, Geneva, 1971). http://dx.doi.org/10.5170/CERN-1971-015

[26] T.O. Raubenheimer and F. Zimmermann, *Phys. Rev*. **E52** (1995) 5487, http://dx.doi.org/10.1103/physreve.52.5487

[27] K. Ohmi, *Phys. Rev*. **E55** (1997) 7550, http://dx.doi.org/10.1103/physreve.55.7550

[28] G. Skripka, R. Nagaoka, M. Klein, F. Cullinan and P.F. Tavares, *Nucl. Instrum. Meth.* **A806** (2016) 221, http://dx.doi.org/10.1016/j.nima.2015.10.029

[29] G. Xia, K. Ohmi and E. Elsen, Simulation study of fast ion instability in the ILC damping ring and PETRA III, unpublished; a revised version by G. Xia and E. Elsen is published in *Nucl. Instrum. Meth* **A593** (2008) 183, http://dx.doi.org/10.1016/j.nima.2008.05.054

[30] J. Byrd, A. Chao, S. Heifets, M. Minty, T.O. Raubenheimer, J. Seeman, G. Stupakov, J. Thomson and F. Zimmermann, *Phys. Rev. Lett.* **79** (1997) 79, http://dx.doi.org/10.1103/physrevlett.79.79

[31] M. Kwon, J.Y. Huang, T.-Y. Lee, I.S. Ko, Y.H. Chin, H. Fukuma, M. Isawa, K. Ohmi and M. Tobiyama, *Phys. Rev*. **E57** (1998) 6016, http://dx.doi.org/10.1103/physreve.57.6016

[32] H. Fukuma, Y. Chin, S. Kato, E. Kikutani, S. Kurokawa, S. Matsumoto, K. Ohmi, Y. Suetsugu, M. Tobiyama, K. Yokoya and X.L. Zhang, Experimental observations of the ion-related coupled bunch instability in a bunch train in TRISTAN AR, PAC97, Vancouver, 1997, p. 1596, http://accelconf.web.cern.ch/accelconf/pac97/papers/pdf/2V009.PDF.

[33] G.V. Stupakov, T.O. Raubenheimer and F. Zimmermann, *Phys. Rev*. **E52** (1995) 5499, http://dx.doi.org/10.1103/physreve.52.5499

[34] K. Ohmi, F. Zimmermann and E. Perevedentsev, *Phys. Rev*. **E65** (2001) 016502, http://dx.doi.org/10.1103/physreve.65.016502

[35] E.S. Kim and K. Ohmi, *Jpn. J. Appl. Phys.* **48** (2009) 086501, http://dx.doi.org/10.1143/jjap.48.086501

[36] S. Sakanaka, The stability of ions in partially filled mode operation in the electron storage ring, KEK Preprint 86-17 (1986).

[37] C.J. Bocchetta and A. Wrulich, *Nucl. Instrum. Meth.* **A278** (1989) 807, http://dx.doi.org/10.1016/0168-9002(89)91205-9

[38] J.A. Clarke, D.M. Dykes, S.F. Hill, E.A. Hughes, M.W. Poole, P.D. Quinn, S.L. Smith, V.P. Suller and L.A. Welbourne, Source size variation and ion effects in the SRS at Daresbury, PAC1993, Washington DC, p. 3594,

http://accelconf.web.cern.ch/AccelConf/p93/PDF/PAC1993_3594.PDF.

[39] B. Schwarzschild, *Phys. Today* March (1986) 19. http://dx.doi.org/10.1063/1.2815138

[40] M. Zobov, A. Battisti, A. Clozza, L. Lollo, C. Milardi, B. Spataro, A. Stella and C. Vaccarezza, *J. Instr*. **2** (2007) P08002, http://dx.doi.org/10.1088/1748-0221/2/08/p08002

[41] H. Zyngier, J.-C. Besson, M. Bordessoule, P. Brunelle, P. Juan, M.-P. Level, P.-C. Marin, P. Nghiem and E.M. Sommer, SUPER-ACO status report, EPAC 1990, Nice, France, p. 469, http://accelconf.web.cern.ch/AccelConf/e90/PDF/EPAC1990_0469.PDF.

[42] K.C. Harkay and R.A. Rosenberg, *Phys. Rev. STAB* **6** (2003) 034402, http://dx.doi.org/10.1103/physrevstab.6.034402

[43] R. Wanzenberg, Observations of electron cloud phenomena at PETRA III, ECLOUD'12 proceedings, Isola d'Elba, 2012, p. 89, http://cds.cern.ch/record/1668184/files/p89.pdf.

[44] M. Izawa, Y. Sato and T. Toyomasu, *Phys. Rev. Lett*. **74** (1995) 5044, http://dx.doi.org/10.1103/physrevlett.74.5044

[45] E. Plouviez, Ph. Arnoux, F. Epaud, J.-M. Koch, G. Naylor and F. Uberto, Bunch by bunch transverse feedback development at the ESRF, EPAC08, Genoa, 2008, p. 3297, http://accelconf.web.cern.ch/AccelConf/e08/papers/thpc132.pdf.

[46] R. Nagaoka, Observation and analysis of fast beam–ion instabilities at SOLEIL, International Workshop on Linear Colliders 2010, Accelerator Working Group 2, CERN, 2010.

[47] K. Oide, cited as private communication in Ref. [26].

[48] M. Kihara *et al*., Results on accelerator studies of the Photon Factory storage ring, KEK 83-5, KEK, Tsukuba, Japan (1983).

[49] M. Kobayashi, K. Huke, S. Ban and H. Hirayama, Observations of Bremsstrahlung caused by ion trapping, Proc. 5th Symp. Acc. Sci. Tech. p. 148, KEK, Tsukuba, Japan (1984).

[50] H. Kobayakawa, K. Huke, M. Izawa, Y. Kamiya, M. Kihara, M. Kobayashi and S. Sakanaka, Observation of ion trapping phenomenon with Bremsstrahlung, KEK Preprint 85-80 (1986).

[51] L. Wang, J. Safranek, Y. Cai, J. Corbett, R. O. Hettel, T. O. Raubenheimer, J. Schmerge and J. Sebek, *Phys. Rev. STAB* **16** (2013) 104402, http://dx.doi.org/10.1103/physrevstab.16.104402

[52] R. Nagaoka, L. Cassinari, M. Diop, J.M. Filhol, M.P. Level, M. Labat, P. Marchand and R. Sreedharan, Study of ion-induced instabilities and transverse feedback performance at SOLEIL, IPAC2011, San Sebastián, Spain, September 201, p. 712, http://accelconf.web.cern.ch/AccelConf/IPAC2011/papers/mops049.pdf.

[53] R. Nagaoka, R. Sreedharan and L. Cassinari, Fast beam-ion instability arising from local outgassing, presented at TWIICE workshop, Synchrotron SOLEIL, Gif-sur-Yvette, France, 2014, http://indico.cern.ch/event/277919/contributions/626920/attachments/506917/699839/05-RNs_talk_TWIICE.pdf.